Limnimeter and Rain Gauge FDI in Sewer Networks using an Interval Parity Equations based Detection Approach and an Enhanced Isolation Scheme

Vicenç Puig, Joaquim Blesa

Advanced Control Systems Group (SAC), Institute of Robotics and Industrial Informatics (IRI-CSIC) ,Universitat Politècnica de Catalunya (UPC), Pau Gargallo, 5 ,08028 Barcelona, Spain
(e-mail: vicenc.puig@upc.edu)

Abstract: In this paper, a methodology for limnimeter and rain-gauge *fault detection and isolation* (FDI) in sewer networks is presented. The proposed model based FDI approach uses interval parity equations for fault detection in order to enhance robustness against modelling errors and noise. They both are assumed unknown but bounded, following the so-called *interval* (or set-*membership*) approach. On the other hand, fault isolation relies on an algorithm that reasons using several fault signature matrices that store additional information to the typical binary one used in standard FDI approaches. More precisely, the considered fault signature matrices contain information about residual fault sign/sensitivity and time/order of activation. The paper also proposes an identification procedure to obtain the interval models used in fault detection that delivers the nominal model plus parameter uncertainty is proposed. To exemplify the proposed FDI methodology, a case study based on the Barcelona sewer network is used.

Keywords: Fault detection, fault isolation, sewer networks, robust methods.

1. INTRODUCTION

Sewer networks are complex large-scale systems which require highly sophisticated supervisory-control systems to ensure that high performance can be achieved and maintained under adverse operating conditions. Most cities around the world have sewage systems that combine sanitary and storm water flows within the same network. This is why these networks are known as *Combined Sewage Systems* (CSS). During rain storms, wastewater flows can easily overload these CSS, thereby causing operators to dump the excess of water into the nearest receiver environment (rivers, streams or sea). This discharge to the environment, known as *Combined Sewage Overflow* (CSO), contains biological and chemical contaminants creating a major environmental and public health hazard. Environmental protection agencies have started forcing municipalities to find solutions in order to avoid those CSO events. A possible solution to the CSO problem would be to enhance existing sewer infrastructure by increasing the capacity of the wastewater treatment plants (WWTP) and by building new underground

1

detention tanks. But, in order to take profit of these expensive infrastructures, a highly sophisticated *real-time control* (RTC) scheme is also necessary which ensures that high performance can be achieved and maintained under adverse meteorological conditions (Schütze, 2004) (Marinaki, 2005). The advantage of RTC applied to sewer networks has been demonstrated by an important number of researchers during the last decades. Comprehensive reviews that include a discussion of some existing implementations are given by (Schilling, 1996) (Schütze, 2004) and cited references therein, while practical issues are discussed by (Schütze, 2002), among other. The RTC scheme in sewage systems might be *local* or *global*. When local control is applied, flow regulation devices use only measurements taken at their specific locations. While this control structure is applicable in many simple cases, in a big city, with a strongly interconnected sewer network and a complex infrastructure of sensors and actuators, it may not be the most efficient alternative. Conversely, a global control strategy, which computes control actions taking into account real-time measurements all through the network, is likely the best way to use the infrastructure capacity and all the available sensor information. The multivariable and large-scale nature of sewer networks has lead to the use of some variants of Model Predictive Control (MPC), as global control strategy (Gelormino, 1994)(Cembrano, 2004)(Pleau, 2005) (Marinaki 2005) (Ocampo-Martínez, 2008).

The global RTC need to operate in adverse meteorological conditions involves, with a high probability, sensor and actuator malfunctions (faults). This problem calls for the use of an on-line *fault detection and isolation* (FDI) system able to detect such faults and correct them (if possible) by activating fault tolerance mechanisms, as the use of soft sensors or using the embedded tolerance of the MPC controller, that avoids that the global RTC should be stopped every time that a fault appears. According to (Schütze, 2004), this is one of the main reasons why today there is a small number of global RTC operating in the world. This difficulty has also been assessed by the author when implementing the global RTC in the Barcelona sewer network (Cembrano, 2004). This has motivated the research presented in this paper.

In the literature, FDI in sewer networks has already been addressed using Takagi-Sugeno multi-models in the case of rain-gauges (Giuliani, 1997) and in the case of limnimeters (Boukhris 1997; 2001). Fault detection is based on checking the residual against a threshold that has been derived either from statistical or empirical approaches. The use of Kalman filters and Wald sequential test has been proposed by (Piatyszek et al., 2000) as means of detecting limnimeter faults in sewer networks. In all these approaches, a simplified deterministic model of rainfall-runoff transformation is considered.

In the present paper, a simplified model based on the virtual tank modelling approach proposed in (Cembrano, 2004) is used to model the rainfall-runoff transformation. This conceptual modelling approach based on establishing mass balances in the sewer

network catchments avoids the complexity of the physical oriented models based on Saint-Venant equations that are not adequate to be used on-line. To consider the uncertainty in the sewer modelling due to the use of this conceptual approach, a FDI approach based on *interval models* and *methods* is proposed (Puig, 2008). Interval methods are very appropriate when the modelling uncertainty is included in the model by means of interval parameters. Moreover, noise can easily handled using the interval methods since only a noise bound is required without any assumption about the statistical distribution. For both reasons, interval methods can be considered as an alternative to *stochastic models* and *methods* (Bassevile and Nikiforov, 2003)(Nikiforov, 1998). In Meseguer (2010), interval observers for fault detection have been already proposed for limnimeter fault detection. In this paper, alternatively interval parity equations expressed in regressor form are proposed. The advantage of interval parity equations with respect to observers is that the algorithm proposed in (Blesa, 2011) for estimating interval parameters and generating detection thresholds can be used. Interval parity approaches are less computational demanding than observers because the parameters enter linearly in the equations. This fact has already noticed by Ploix and Adrot (2006) .

In this paper, the problem of FDI is mainly focused on rain gauges and limnimeters used for the RTC of a sewer network, but could easily being extended to actuator faults or faults in other elements in the network. The proposed fault detection and isolation strategy is based on building an interval model for every instrument. Then, each instrument reading is compared with the prediction provided by its interval model. While, the real measurement is inside the interval of predicted behaviour (or envelope) generated using its interval model, no fault can be indicated. However, when the measurement is outside its envelope, a fault can be indicated (Puig, 2008). Once the fault has been detected, a fault isolation procedure is initiated in order to isolate the faulty instrument. The proposed FDI approach introduces also an improved interface between fault detection and isolation that reasons not only using binary information about fault signal activation but also considers residual fault sensitivities and time/order of activation. The need of such improved interface has been motivated because the application of the standard binary interface between fault detection and isolation could lead to wrong diagnosis when the residuals present different sensitivities and order/time of activation after the fault appearance (Combastel, 2003). The proposed diagnosis approach in this paper comes from an evolution of the algorithm presented in (Puig, 2005). In the literature, there have also appeared other proposals following the same spirit as the one proposed by (Van den Daele *et al*., 1997) where the activation of a residual generates an event with a belief and time stamp, among other attributes. Then, a reasoning using a causal graph produces a set of candidate faults ranked from the most to the least probable. In the same line, (Ragot, 2006) proposed an improved fault diagnosis approach based on the fuzzy evaluation of the residuals that considers not only binary information but also signs/sensitivities as well as the persistence of residual activation. This approach has also been applied to a water network.

96

97   To exemplify the FDI problem in sewer networks and the proposed FDI methodology, the Barcelona network is used as the

98   case study. Such network has a telemetry system containing 22 rain gauges and more than 100 limnimeters used for the RTC

99   system. In this paper, a representative part of this network is considered.

100

101   The organisation of the paper is the following: *Section 2* presents how models for FDI in rain-gauges and liminimeters are built

102   and intervals for parameters are estimated. *Section* 3 overviews the proposed FDI scheme. *Section 4* and *5* discuss the

103   implementation of the fault detection and isolation modules. *Section 6* presents a description of the Barcelona sewer network

104   used as a case study and shows the results obtained using the proposed FDI scheme. Finally, *Section 7* closes the paper with

105   the conclusions.

106

107   2. INTERVAL MODELS FOR FDI IN SEWER NETWORKS

108

109   Rain gauges and limnimeters are the two type of sensors used in the RTC of sewer networks: the first type measures rain

110   intensity while the second one measures the sewer water level. In general, when detecting faults in sensors two strategies are

111   possible: *hardware redundancy* based on the use of redundant (extra) sensors and *analytical redundancy* based on the use of a

112   mathematical model that combines measurements from other correlated sensors or from the same sensor in past instants

113   (Patton, 2000). In critical systems (space aircrafts, aeroplanes, ...) hardware redundancy is preferred. But, in large scale

114   systems (as the case of sewer networks), the use of hardware redundancy is very expensive and increases the number of

115   maintenance and calibration operations. That is the reason why analytical redundancy has been proved to be a good and

116   cheaper alternative. This is the approach followed in this paper.

117

118   *2.1 Modelling limnimeters*

119

120   Typically, in sewer networks, sewage level is measured instead of flow. There are two reasons that can explain this fact. First

121   since the level is measured using ultrasonic waves, limnimeters do not have contact with the sewage flow (Fig. 1), and

122   consequently, the required maintenance is cheaper. Second, limnimeters are cheaper than flowmeters. Ultrasonic limnimeters

123   generates an acoustic pulse that is transmitted from the transducer and then it is reflected back from the surface of the liquid.

124   The transit time is then converted into the current output, which is directly proportional to the fluid level. From level

125   measurements, the flow in a sewer can be estimated assuming steady-uniform flow and using the Manning formula calibrated

126   using experimental data (Duchesne, 2001). However, as also discussed in (Duchesne, 2001), where there is not enough slope

127   in the sewer, the backwater effect could appear leading to a complex relation between flow and level that can not be explained

128   by a static relation as the Manning formula. In the sewer network locations where the backwater effect is important, the use of

129   a flow meter instead of a limnimeter is advisable.

130

131   Limnimeters can be monitored in rain scenarios[1] using an on-line rainfall-runoff model of the sewer network that characterizes

132   the net rainfall entering as flow in the sewers. The water flow in sewers due to runoff is open-channel. The Saint-Venant

133   equations, based on physical principles of mass conservation and energy, allow describing accurately the open-channel flow in

134   a sewer (Marinaki, 2005). Such complex non-linear rainfall-runoff models are very useful for off-line operations (calibration

135   and simulation) of the sewer network. But for on-line purposes, as the global optimal control and FDI, a simpler conceptual

136   model must be used (Duchesne, 2001). One possible modelling methodology to derive a rainfall-runoff real-time model of a

137   sewer network is based on using a simplified graph relating the main sewers and catchments as a set of virtual reservoirs

138   (Cembrano, 2004).

139

140

141

142   Fig. 1. Limnimeter inside a sewer

143

144   A *virtual reservoir* is an aggregation of a sewer capacity in a catchment of the sewer network which approximates the

145   hydraulics of rain infiltration, runoff and sewage water retention thereof (Fig. 2).

146

---

[1] In dry scenarios, to monitor limnimeters a different modelling approach (based on time series) could be used to exploit the temporal redundancy existing in the sensor measurements. These measurements follow the patterns of consumer drinking water demands with daily and weekly cycles as the flow meters in a drinking water network. In Quevedo et. al (2010), an approach to detect faults in flow meters in a drinking water network.
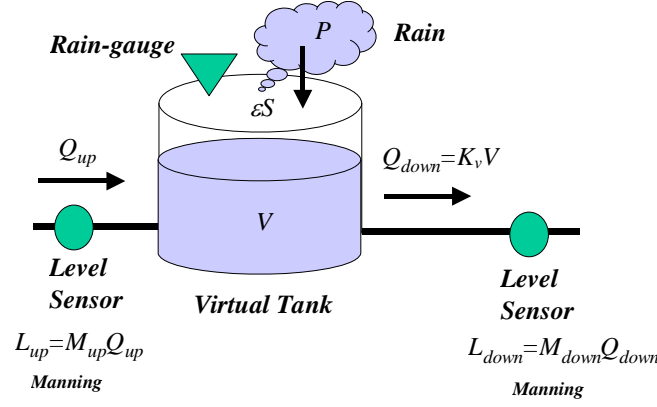
Fig. 2. Virtual reservoir model of a catchment

The hydraulics of a virtual reservoir that models a catchment is given by

$$\frac{dV(t)}{dt} = Q_{up}(t) - Q_{down}(t) + \varepsilon P(t)S \tag{1}$$

where: V is the volume of water accumulated in the catchment, Q_{up} and Q_{down} are flows entering and exiting the catchment, P is the rain intensity falling in the catchment, S its surface and ε the ground absorption coefficient. Upstream and downstream sewage levels (L_{up}, L_{down}) are measured using limnimeters and they can be related with upstream/downstream flows (Q_{up}, Q_{down}) using a linearised Manning relation:

$$Q_{up}(t) = M_{up}L_{up}(t) \tag{2}$$

$$Q_{down}(t) = M_{down}L_{down}(t) \tag{3}$$

where M_{up}, M_{down} are the limnimeter Manning coefficients estimated experimentally.

It is additionally assumed that the catchment behave as a linear virtual tank, i.e., that a linear relation between the volume of the water stored in the virtual tank is linearly related with the flow downstream the catchment

$$Q_{down}(t) = K_v V(t) \tag{4}$$

where K_v is the volume/flow conversion coefficient estimated experimentally as well.

Then, substituting (4) in (1) and discretising using the Euler method with a sampling time Δt, the following discrete-time relation (k is the discrete time) between upstream and downstream flows can be derived:

$$Q_{down}(k+1) = (1 - K_v\Delta t)Q_{down}(k) + K_v\Delta t Q_{up}(k) + K_v\Delta t \varepsilon SP(k)) \tag{5}$$

169 Finally, replacing (2) and (3) in (5), leads to the following relation between upstream and downstream limnimeter

170 measurements

$$L_{down}(k+1) = aL_{down}(k) + bL_{up}(k) + cP(k))$$ (6)

173 where:

$$a = (1 - K_v \Delta t), \quad b = \frac{M_{up} K_v \Delta t}{M_{down}} \quad \text{and} \quad c = \frac{K_v \Delta t \varepsilon S}{M_{down}}$$

176 *2.2 Modelling rain-gauges*

178 Typical rain-gauges used in sewer networks are of tipping bucket type (see Figure 3(a)). This gauge technology uses two small

179 buckets mounted on a fulcrum (balanced like a see-saw) (see Figure 3(b)). The tiny buckets are manufactured with tight

180 tolerances to ensure that they hold an exact amount of precipitation. The tipping bucket assembly is located above the rain

181 sewer, which funnels the precipitation to the buckets. As rainfall fills the tiny bucket, it becomes overbalanced and tips down,

182 emptying itself as the other bucket pivots into place for the next reading. The action of each tipping event triggers a small

183 switch that activates the electronic circuitry to transmit the count to the indoor console, recording the event as a given number

184 of *mm/h* of rainfall. The number of tipping events in a pre-established sampling time is accumulated and multiplied by a factor

185 in order to obtain the rain intensity in *m/s* at each sampling time, after the appropriate unit conversion.

188 (a) (b)
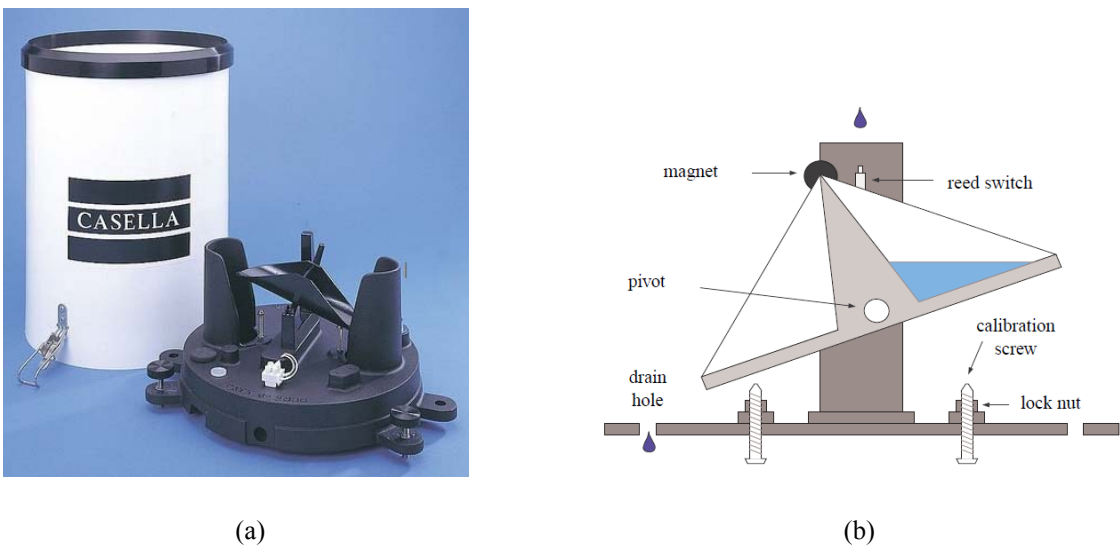
189 Fig. 3. (a) A rain-gauge manufactured by Casella Measurement and (b) Principle of operation of a tipping bucket rain-gauge

191   In order to detect faults in a given rain-gauge P_i, a model that exploits *spatial redundancy* existing in the rain-gauge network is

192   used. The model relates the measurements of rain-gauge P_i with the m most-correlated rain-gauges ($P_1,...,P_m$) at time instant k

193   as follows

194    $$P_i(k) = \alpha_1 P_1(k) + \alpha_2 P_2(k) + ... + \alpha_m P_m(k)$$ (7)

195   The most correlated rain-gauges correspond to the ones that are the closest in distance as discussed in (*Figueras* et al., 2005).

196
197   *2.3   Estimation of interval models*

198

199   One of the key points in using the interval model based fault detection is how intervals of model parameters are estimated from

200   scenarios free of faults. The estimation process should deliver a nominal model plus its modelling error in the form of interval

201   parameters that will provide an interval of confidence for the predicted behaviour. Several authors ((Ploix, 1999) (Calafiore,

202   2002)(Campi, 2009)) have suggested an adaptation of standard system identifications methods to provide the nominal model

203   plus the uncertainty intervals for parameters that guarantee that all recorded data from the system in non-faulty scenarios will

204   be included in the interval model. These algorithms are based on using standard identification methods (for example, least-

205   squares) to provide the nominal estimate for system parameters. Then, the intervals of uncertainty for parameters are adjusted

206   until all the measured data is covered by the model prediction interval.

207

208   The algorithm proposed in this paper considers that the interval model to be identified can be expressed in regressor form as

209   follows

210    $$y(k) = \boldsymbol{\varphi}(k)\boldsymbol{\theta}(k) + e(k)$$ (8)

211   where: $\varphi(k)$ is the regressor vector of dimensions $1 \times n_\theta$ which can contain any function of inputs ($u(k), u(k-1), u(k-2), ...$)

212   and outputs ($y(k), y(k-1), y(k-2), \cdots$), $e(k)$ is additive noise bounded by a constant $|e(k)| \leq \sigma$, $\boldsymbol{\theta}(k) \in \boldsymbol{\Theta}$ is the parameter

213   vector of dimensions $n_\theta \times 1$ and $\boldsymbol{\Theta}$ is an interval box centred in the nominal parameter values $\boldsymbol{\Theta} \triangleq [\theta_1] \times \cdots \times [\theta_i] \times \cdots \times [\theta_{n_\theta}]$

214   where $[\theta_i] \triangleq [\theta_i^0 - \lambda_i, \theta_i^0 + \lambda_i]$, $i=1,...,n_\theta$, with θ_i^0 being the nominal parameter values and $\lambda_i \geq 0$ the parameter

215   uncertainties. The uncertain interval parameter set $\boldsymbol{\Theta}$ can be parameterised as a particular case of a zonotope (Blesa et al,

216   2011) as follows:

217    $$\boldsymbol{\Theta} = \left\{ \boldsymbol{\theta}^0 + \mathbf{H}\mathbf{z} : \mathbf{z} \in \mathbf{B}^n \right\}$$ (9)

218   with centre $\boldsymbol{\theta}^0$ and matrix uncertainty shape $\mathbf{H}$ equal to a $n_\theta \times n_\theta$ diagonal matrix:

219    $$\boldsymbol{\theta}^0 = \begin{pmatrix} \theta_1, & \theta_2, & \cdots, & \theta_{n\theta} \end{pmatrix}$$

8

220
$$\mathbf{H} = diag\left(\lambda_1, \lambda_2, ..., \lambda_{n_\theta}\right)$$

221 and $\mathbf{B}^n \in \mathbb{R}^{n \times 1}$ is a unitary box composed by n unitary ($\mathbf{B} = [-1,1]$) interval vectors where $n = n_\theta$.

222

223 Then, proceeding as in Blesa et al (2011), the maximum and minimum values of the prediction provided by model (8) with

224 uncertain parameter set (9) are given by

225
$$\overline{\hat{y}}(k) = \hat{y}^0(k) + \left\|\mathbf{H}\boldsymbol{\varphi}(k)\right\|_1 \qquad (10)$$

226
$$\underline{\hat{y}}(k) = \hat{y}^0(k) - \left\|\mathbf{H}\boldsymbol{\varphi}(k)\right\|_1 \qquad (11)$$

227 where $\hat{y}^0(k)$ is the model output prediction with nominal parameters: $\hat{y}^0(k) = \boldsymbol{\varphi}(k)\boldsymbol{\theta}^0$. In the particular case of interval

228 parameters: $\left\|\mathbf{H}\boldsymbol{\varphi}(k)\right\|_1 = \sum_{i=1}^{n} \lambda_i \left|\varphi_i(k)\right|$.

229 Then, given a sequence of data in a fault free scenario (measurements of regressor vector $\boldsymbol{\varphi}(k)$ and output $y(k)$ for

230 $k = 1, ..., N$) and rich enough from the identifiability point of view, the estimation problem boils down in determining the

231 nominal parameter vector ($\boldsymbol{\theta}^0$) and the parameter uncertainty (defined by matrix $\mathbf{H}$) in such a way that all the measurements

232 are inside the prediction interval (given by bounds (10) and (11)) and, the size of intervals for parameters is minimised.

233 The identification of $\boldsymbol{\theta}^0$ and $\mathbf{H}$ can be carried out in two steps: In the first step, nominal vector parameter can be identified

234 (by conventional methods, i.e least squares). Then, in the second the parameter uncertainties defined by $\mathbf{H}$ can be computed.

235 From equations (10) and (11), the smallest intervals for parameters that satisfy $y(k) \in \left[\underline{\hat{y}}(k), \overline{\hat{y}}(k)\right]$ for $k = 1, ..., N$ can be

236 computed solving the following optimization problem

237
$$\min_{\mathbf{H}} vol(\boldsymbol{\Theta}(\mathbf{H}))$$

238 subject to: $\qquad \hat{y}^0(k) + \left\|\mathbf{H}\boldsymbol{\varphi}(k)\right\|_1 \geq y(k) - \sigma \qquad\qquad k = 1, ..., N \qquad (12)$

239 $\qquad\qquad\qquad\qquad\qquad \hat{y}^0(k) - \left\|\mathbf{H}\boldsymbol{\varphi}(k)\right\|_1 \leq y(k) + \sigma$

240

241 In order to reduce the complexity of the optimization problem (12), the uncertain parameter set $\boldsymbol{\Theta}$ can be parameterised such

242 that a pre-determined shape $\mathbf{H}_0$, as proposed in Blesa et al (2011), is used. The shape $\mathbf{H}_0$ can be estimated, for example,

243 from the parameter variance of estimated nominal model: $\mathbf{H} = \lambda \mathbf{H}_0$. Other heuristics could also be used (for more details see

244 Blesa et al (2011)).

245 In the case of considering $\mathbf{H} = \lambda \mathbf{H}_0$, the optimal solution of (12) is provided by:

9

246

$$\lambda = \sup_{k \in \{1,...,N\}} \left(\frac{\left| y(k) - \hat{y}^0(k) \right| - \sigma}{\left\| \boldsymbol{\varphi}(k) \mathbf{H}_0 \right\|_1} \right) \tag{13}$$

248

3. OVERVIEW OF THE PROPOSED FDI SCHEME

250

3.1 Introduction

The standard FDI scheme is based on generating a set of numerical fault indicators, known as *residuals* which are computed using analytical redundancy relations (obtained from model equations) and the measured inputs and outputs of the monitored system. Then, the fault detection task consists in deciding if there is a fault affecting the monitored system by checking each residual against a threshold that takes into account model uncertainty, noise and the unknown disturbances. The result of this test applied to every residual produces an *observed fault signature*. The observed fault signature is supplied to the fault isolation module that will try to isolate the fault by looking at theoretical binary fault signature matrix where a binary relation between the considered fault hypothesis set. However, when applying this standard FDI scheme to limnimeters and rain-gauges in sewers networks, the following drawbacks were noticed:

(a) The detection threshold should be determined and adapted on-line according to the system inputs and outputs taking into account the model uncertainty.

(b) The presence of the noise produces chattering if a binary evaluation of the residual is used.

(c) All residuals affected by a certain fault should be activated at the same time instant and they should be persistently keeping activated during the whole fault isolation process. Otherwise, a wrong fault diagnosis result could be given.

(d) Restricting the relation between faults and fault signals to a binary one causes a loss of useful information that can add fault distinguishability and accurateness to the fault isolation algorithm preventing possible wrong fault diagnosis results.

267

3.2 Proposed FDI scheme

269

To deal with the previous issues, the FDI scheme, presented in Figure 4, is proposed. This scheme is composed of different modules that play the following role (Fig. 4):

272

10

273   -   *Fault detection module* is based on evaluating the residual against an adaptive threshold generated evaluating the

274   interval parity equations that evolves along time taking into account model uncertainty and noise (Puig, 2008) (see

275   *Section 4* for more details).

276   -   *Fault detection/isolation interface module* evaluates fault signals generated by the fault detection module in order to

277   isolate the fault among the considered fault hypotheses using several indicators which take into account not only the

278   activation value of the fault signal but also its fault sensitivity/sign and its activation time/order. This improved

279   interface module try to handle the problems associated with the fault signal persistency, the residual sensitivity to a

280   fault, the fault signal occurrence order and the fault signal occurrence time instant (see *Section 4 and Appendix 1* for

281   more details).

282   -   *Fault isolation module* reasons with the information provided by all the indicators/fault signature matrices to achieve

283   the fault isolation (see *Section 5* for more details).

284 The underlying assumptions considered in the proposed FDI approach are that no multiple faults ("*single fault hypothesis*")

285 and faults can be modelled in an additive way as in the standard FDI approaches (Gerlter, 1998).
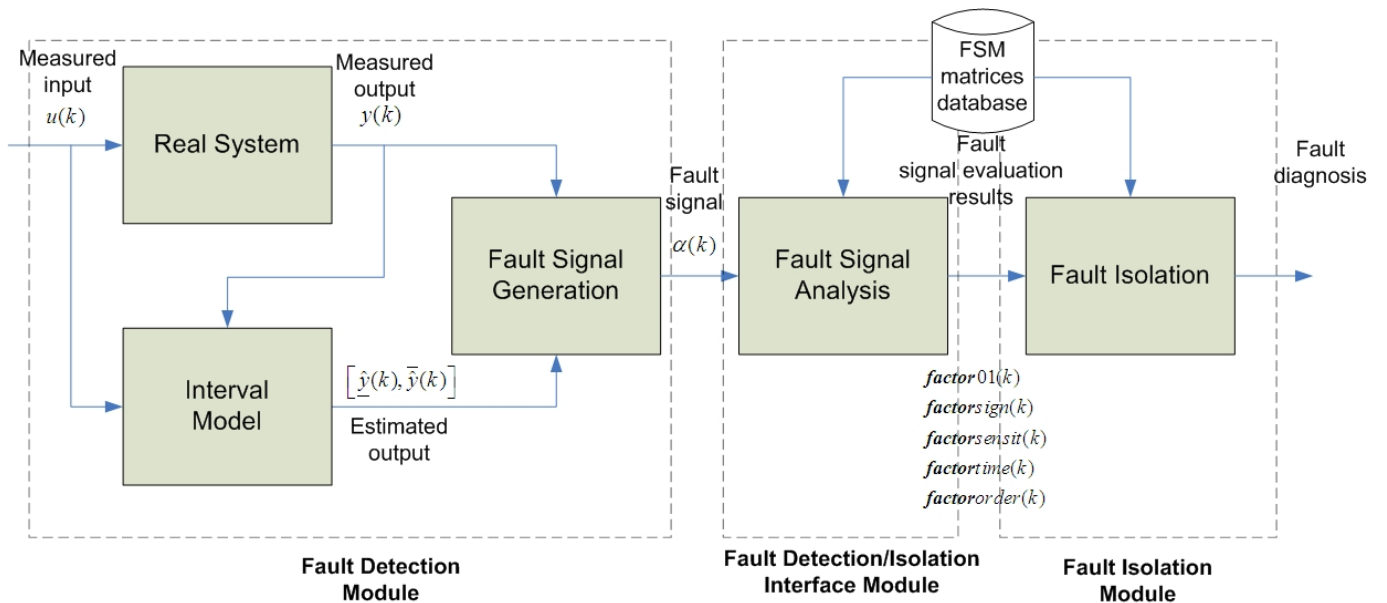

287 Fig. 4. FDI proposed scheme

288

289   4. FAULT DETECTION MODULE AND INTERFACE WITH FAULT ISOLATION MODULE

290

291 *4.1 Fault detection module*

292 The fault detection module is based on the evaluation of the nominal residual obtained from difference between measurements

293 and model prediction using model in regressor form (8)

11

294
$$r^o(k) = y(k) - \hat{y}^o(k) = y(k) - \mathbf{\phi}(k)\mathbf{\theta}^o \qquad (14)$$

295   where $\mathbf{\theta}^o$ are the nominal parameters.

296   Taking into account parametric modelling errors, the detection test consists in evaluating the following condition

297
$$r_i^o(k) \in \left[\underline{r}_i^o(k), \overline{r}_i^o(k) \right] \qquad (15)$$

298   where: $\underline{r}_i^o(k) = \underline{\hat{y}}_i(k) - \hat{y}_i^o(k)$ and $\overline{r}_i^o(k) = \overline{\hat{y}}_i(k) - \hat{y}_i^o(k)$ while $\underline{\hat{y}}_i(k)$ and $\overline{\hat{y}}_i(k)$ are the bounds of the ith-system output
299   prediction calculated using (10) and (11).
300

301   Test condition (15), equivalently, can be expressed as follows:

302

303
$$y_i(k) \in \left[\underline{\hat{y}}_i(k), \overline{\hat{y}}_i(k) \right] \qquad (16)$$

304   *4.2 Mininum detectable*

305   The effect of faults in the residual can be expressed in terms of the residual fault sensitivity that leads to the residual internal

306   form (Gertler, 1998). In case of considering additive input (f_u) and output (f_y) sensor faults, the computational form of the

307   residual (14) can be expressed as follows:

308
$$r^o(k) = S_{f_y}(q^{-1})f_y(k) + S_{f_u}(q^{-1})f_u(k) \qquad (17)$$

309   where $S_{f_y}(q^{-1})$ and $S_{f_u}(q^{-1})$ are the residual fault output and input sensitivity transfer functions. Considering residual (14),

310   the sensitivities are given by: $S_{f_y}(q^{-1}) = 1 - \dfrac{\partial \mathbf{\phi}(k)}{\partial f_y}\mathbf{\theta}^0$ and $S_{f_u}(q^{-1}) = -\dfrac{\partial \mathbf{\phi}(k)}{\partial f_u}\mathbf{\theta}^0$.

311   According to Gertler (1998), the *minimum detectable fault* $f_i^{\min}(k)$ corresponds to a size of fault that brings a residual (15) to

312   its threshold (*"triggering limit"*), assuming that no other faults and nuisance inputs are present.

313   When using the fault detection (16) (or (15), a fault $f(k)$ will always be detected when its fault effect ($\delta_f(k)$) is bigger than

314   the interval prediction thickness ($\delta_r(k)$). In the case of using model (8) with parameters (9), they can be computed according

315   to (Blesa *et al.*, 2011) as follows: $\delta_f(k) = S_f(q^{-1})f(k)$ and $\delta_r(k) = 2\|\mathbf{\phi}(k)\mathbf{H}\|_1 + 2\sigma$ where $S_f(q^{-1})$ is the residual fault

316   sensitivity transfer function that characterizes the effect of fault in the residual. Then the minimum detectable fault can be

317   computed as

318
$$\left| f_f^{\min}(k) \right| = \frac{2\|\mathbf{\phi}(k)\mathbf{H}\|_1 + 2\sigma}{\left| S_f(q^{-1}) \right|} \qquad (18)$$

319   Notice that minimum detectable fault defined by Eq. (17) is not a constant value, but a value that evolves dynamically and

12

320   depends on the operation point (defined by $\boldsymbol{\varphi}(k)$). Then, the *minimum steady state detectable fault* can be obtained considering

321    $S_f(q^{-1})|_{q=1}$ in Eq (18). Analogously, the *minimum initial detectable fault* can be obtained considering $S_f(q^{-1})|_{q\to\infty}$ in (18).

322

323   *4.2 Interface between fault detection and isolation*

324

325   The fault detection test (16) relies on the comparison of the nominal residual $r_i^o(k)$, which may be affected by noise, with its

326   associated adaptive threshold (interval $[\underline{r}_i^o(k), \overline{r}_i^o(k)]$). This binary procedure may lead to undesirable decision instability

327   (chattering) because of the effect of noise on the sensor measurements. Such as indicated by the DMP-approach (Petti et al.,

328   1990), a gradual reasoning based on the use of fuzzy evaluation is an appealing alternative to bypass this chattering

329   phenomenon. Then, the *fault diagnostic signal* (or *fault signal*) for each residual is calculated in the approach presented in this

330   paper using the Kramer function (Petti et al., 1990):

331
$$\phi_i(k) = \begin{cases} \dfrac{(r_i^o(k)/\overline{r}_i^o(k))^4}{1+(r_i^o(k)/\overline{r}_i^o(k))^4} & if \quad r_i^o(k) \geq 0 \\[4mm] -\dfrac{(r_i^o(k)/\underline{r}_i^o(k))^4}{1+(r_i^o(k)/\underline{r}_i^o(k))^4} & if \quad r_i^o(k) < 0 \end{cases} \tag{19}$$

332   The appealing performance of this function is due to the grading that introduces when evaluating the residual in order to

333   conclude about the fault existence. When using Eq. (19), the residuals are normalized to a metric between -1 and 1,

334    $\phi_i(k) \in [-1,1]$, which indicates the degree of satisfaction of Eq. (16) for every nominal residual $r_i^o(k)$: *0* for perfectly

335   satisfied, *1* for severely violated high and *-1* for severely violated low.

336

337   5. FAULT ISOLATION MODULE

338

339   The fault isolation module used in this paper derives from the one used proposed in (Puig et al., 2005) (see Figure 5). The first

340   component is a memory that stores information about the fault signal occurrence history and the fault detection module updates

341   it cyclically. The pattern comparison component compares the memory contents with the stored fault patterns. The standard

342   Boolean fault signature matrix concept (Gertler, 1998) is generalized taking into account more fault signal properties. The last

343   component represents the decision logic part of the method which aim is to propose the most probable fault candidate.
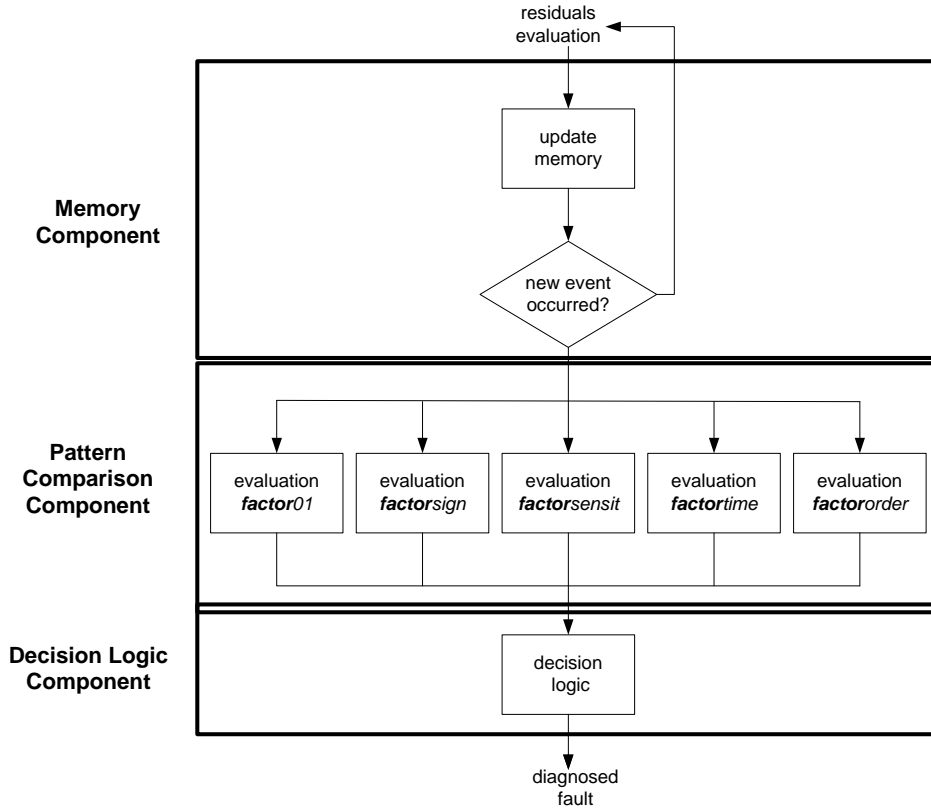
Fig. 5. Fault isolation module components

344

345

346

347 *5.1 Memory component*

348

349 The memory component consists of a table in which events in the residual history are stored. For each row, the first column

350 stores the event occurrence time t_i, the second one stores the *maximum activation value* $\phi_{i,\max}$ computed according to

351
$$\phi_{i,\max} = \max_{k \in [k_o, k_o + T_w]} \left(|\phi_i(k)| \right) \tag{20}$$

352 for every fault signal, and the last one stores the *sign* of the residual. Fault signals with $|\phi_{i,\max}| < 0.5$ are filtered out. Using this

353 strategy the effect of noise and non-persistent fault indicators are filtered because just the peaks of activation are stored. If the

354 fault detection component detects a new residual event (that is, $|\phi_i(k)| \geq 0.5$), the memory component table is updated by

355 adding a new row that contains all previous event information. The problem of different time instant appearance of fault

356 signals $\phi_i(k)$ is solved not indicating the isolation decision until a prefixed waiting time T_w has elapsed from the first fault

357 signal appearance. This T_w is calculated from the larger transient time response T_{lt} from non-faulty situation to any faulty

358 situation. After this time has elapsed, a diagnosis is proposed and the memory component is reset being ready to start the

359 diagnosis of a new fault. Inside this diagnosis window, the maximum activation value of the memory-table $\phi_{i,\max}$

14

360 corresponding to residual i changes only if the current activation value $\phi_i(k_0)$ is superior to the previous ones according to

361 (20).

362

363 *5.2 Pattern comparison component*

364

365 The pattern comparison component compares the memory contents with the stored fault patterns. Given a set of residuals, r_i^0,

366 and the considered set of faults $F = \{f_1, f_2, ..., f_j, ... f_m\}$, each r_i^0 is affected by a subset of these faults. The fault patterns are

367 organized according to a theoretical fault signature matrix, named **FSM**. An element **FSM**$_{ij}$ of the matrix contains the pattern if

368 f_j is expected to affect r_i^0, otherwise, it is equal to 0. This interpretation assumes that the occurrence of f_j is observable in r_i^0,

369 hypothesis known as *fault exoneration* or no *compensation*, and that f_j is the only fault affecting the monitored system. Five

370 different fault signature matrices are considered in the evaluation task: Boolean fault signal activation (**FSM**01), fault signal

371 signs (**FSM**sign), fault residual sensitivity (**FSM**sensit), and, finally, fault signal occurrence order (**FSM**order) and time

372 (**FSM**time). Theses matrices can be obtained from the analysis of residual fault sensitivity (17). Details on how the general

373 rules to obtain those matrices from (19) are derived can be found in (Meseguer, 2007;2009). In the *Appendix 2*, the detailed

374 definition and usage of these matrices is presented.

375

376 *5.3 Decision logic component*

377

378 The decision logic algorithm starts when the first residual is activated (that is, $|\phi_i(k)| \geq 0.5$) and lasts T_w time instants or till all

379 fault hypotheses except one are rejected because they do not fulfil the observed residual activation order/time or because an

380 unexpected activation signal has been observed according to those fault hypotheses. Rejection is based on using the results of

381 *factor01$_j$*, *factorsign$_j$* and *factororder$_j$*. That is the case, if any of these factors is 'zero' for a given fault hypotheses, it will be

382 rejected. Every factor represents some kind of filter, which only lets slip through the possible fault hypotheses. At the end of

383 the time window T_w, for each non-rejected fault hypothesis, a fault isolation indicator is calculated using the factors

384 *factorsensit$_j$* and *factortime$_j$*. Thus, the biggest fault isolation indicator will determine the diagnosed fault. The fault isolation

385 indicator associated to the fault hypothesis f_j is determined as it follows:

386

387 $$d_j = \max(\left|\boldsymbol{factorsensit}_j\right|, \boldsymbol{factortime}_j) \tag{21}$$

388

389   So, the final diagnosis result can be expressed as a set of fault candidates with their associated fault isolation indicator.

390

391   *5.4 Comparison with existing approaches*

392   The fault isolation approach presented in this paper has been compared in (Puig, 2005) with other approaches commonly used

393   in the literature, namely:

394   • the standard FDI binary approach (Gertler, 1998) based on looking for a column of the fault signature matrix that

395   matches the observed fault signature (called *column reasoning* in Cordier *et al.* (2004))

396   • the DX approach based of reasoning only with the activated fault signals and the corresponding rows of the fault

397   signature matrix (called *row reasoning* in Cordier *et al*, (2004),

398   • the DMP approach proposed by Petti *et al.* (1990) that only reasons with the fault residual sensitivity (**FSM**sensit) and

399   • the DTS approach proposed by Kóscielny (1995) that uses the knowledge about the times in which fault signal should

400   be activated after the fault is detected. This approach looks at a row of the fault signature matrix only after its fault

401   signal detection time has elapsed (similar to row reasoning approach). But, in this way it is looking step-by-step at all

402   rows, counting ones and zeros (similar to column reasoning approach).

403   The comparison in Puig et *al.* (2005) has been done using the well known two tank system described in Blanke et *al.* (2006),

404   considering six different faults in scenarios with different fault sizes. Two performance criteria have been used for comparison:

405   • The *diagnostic resolution* defined as the average number of valid fault hypotheses per diagnosis, and the best possible

406   value is 1.

407   • The *diagnostic error rate* defined as the average percentage of wrong diagnoses. An error rate of 0 is desirable.

408   Thus, the optimal point in the error rate/diagnostic resolution-plane is (0/1). Figure 6 shows how the different methods are

409   positioned in this plane. It can be noticed that the proposed method is the one that approaches the most to the optimal point.

16

410
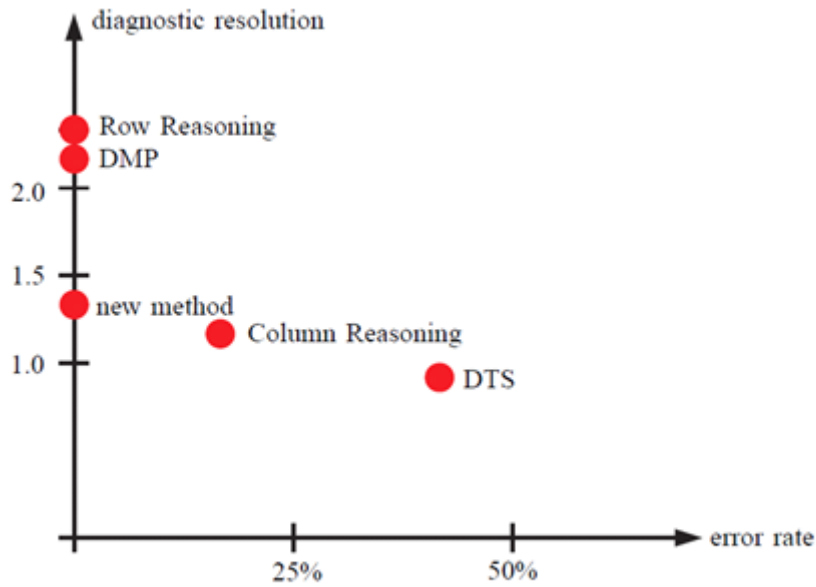
411   Fig. 6. Comparison of the proposed approach with commonly used

412   approaches in the error rate/diagnostic resolution-plane

413

414   *5.5 Extension to address multiple faults*

415   In section, some ideas on how the proposed method could be extended to deal with the multiple faults case. As discussed in

416   Koscielny (2003), when dealing with multiple faults two types of situations are considered depending if the faults appear in

417   *simultaneous* or *sequential* way. In order to use the proposed fault isolation approach in case of simultaneous faults (i.e., faults

418   that appear in a time smaller than the waiting time T_w) two cases can be considered:

419   -   in case the fault signals do not present different time of appearance, the fault signature matrices should be extended

420   adding extract columns to consider the case of multiple faults as in the standard FDI approach (see Gertler, 1998).

421   More precisely, a new column for each combination of possible multiple fault to be considered should be added.

422   -   on the other hand, if the fault signals present different time of appearance, the diagnostic inference may fail if two or

423   more faults occur at a time interval that is shorter than the time window T_w needed for diagnosis. So this situation is

424   not supported by the algorithm.

425   Finally, in case of sequential faults (i.e., faults that appear in a time bigger than the waiting time T_w), the approach can be used

426   under the assumption of single faults, but reconfiguring the fault signature matrices by removing the faulty sensors and the

427   residual expressions where they appear should be derived again. For more details see Figureras *et al*, (2005).

428

17

429

430

431   6. APPLICATION TO THE BARCELONA SEWER NETWORK

432

433   *6.1 Description*

434   The city of Barcelona, with a population of around 1.593.000 inhabitants living on a surface of 98 Km^2 approximately, has a

435   combined sewage system of approximately 1697 Km length with a storage capacity of 3.038.622 m^3. It is a unitary system that

436   combines waste and rainwater into the same sewers. The yearly rainfall is not very high (600 mm/year), but it includes heavy

437   storms (arriving to 90 mm/h) typical of the Mediterranean climate that can cause a lot of flooding problems and combined

438   sewer overflow (CSO) to the receiving environment. Clavegueram de Barcelona, S.A. (CLABSA) is the company in charge of

439   the sewage system management. Nowadays, for control purposes, the urban drainage system contains 21 pumping stations, 36

440   gates, 10 valves and 10 detention tanks which are regulated in order to prevent flooding and to CSO the environment. The

441   remote control system is equipped with 56 remote stations including 22 rain-gauges and 136 water-level sensors which provide

442   real-time information (every 5 minutes) about rainfall and water levels into the sewer system. All this information is

443   centralized at the CLABSA Control Centre through a Supervisory Control and Data Acquisition (SCADA) system. The

444   regulated elements (pumps, gates and detention tanks) are currently controlled locally, i.e., they are handled from the remote

445   control centre according to the measurements of sensors connected only to the local station.

446

447   *6.2 FDI in limnimeters*

448

449   *6.2.1 Introduction*

450   In order to show the proposed FDI methodology in liminimeters, a representative portion of the Barcelona sewer network is

451   studied. The considered portion has a surface of 22,6 Km^2 and is constituted by 11 catchments. The considered part of the

452   network can be analysed separately from the rest of the network. In this part of the network there are 15 level gauges

453   (limnimeters) and 4 rain-gauges. Using the virtual tank modelling methodology presented in *Section 2.1*, a model for this part

454   of the network is presented in Figure 7 where every catchment is represented by a virtual tank. The structure of the model

455   comes from the network physical topology.   The models of each liminimeter (L_3, L_7, L_8, L_9, L_{16}, L_{19}, L_{27}, L_{39}, L_{41}, L_{45}, L_{54}, L_{56}

456   and L_{80}) come from the application of Eq. (5) to the virtual tanks appearing in Figure 7[2]. Figure 8 shows the Boolean fault

---

[2] The weirs appearing in Figure 7 in the considered fault scenarios are not overflowing. This is the reason why in the limnimeter models, the overflowing

paths have not been considered. If overflowing paths are considered, the structure of the limnimeter models would change. This means that the behaviour of

457   signature matrix (**FSM**01) corresponding to set of residuals that are obtained from the liminimeter models. The other fault

458   signature matrices (**FSM**sign, **FSM**sensit, **FSM**order and **FSM**time) are obtained from the analysis of residual fault sensitivity

459   (19), as discussed in *Section 5.3*, as described in (Meseguer, 2007;2009). In *Appendix 2*, the content of these matrices is
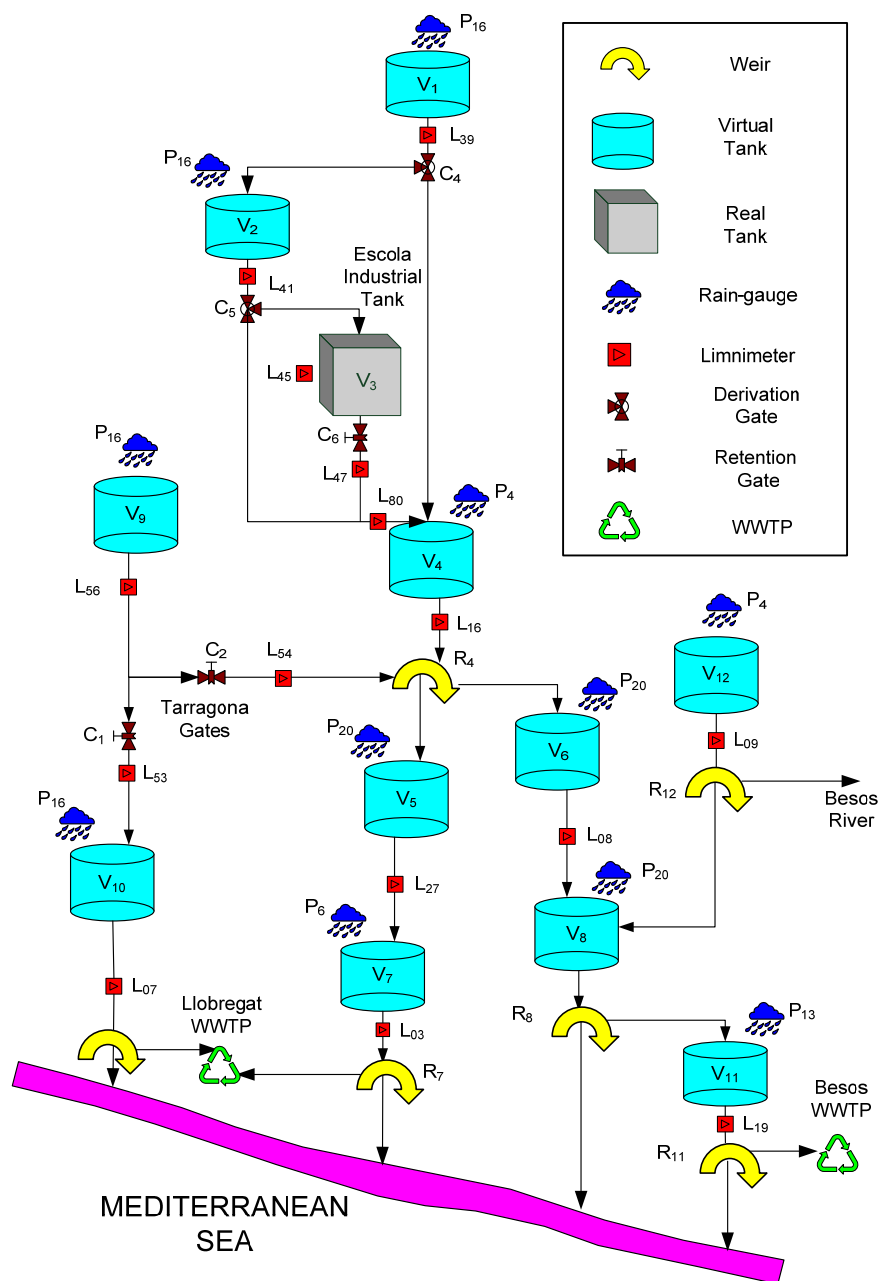
460   presented for this application.

461

462   Fig. 7. Virtual reservoir model of the portion of Barcelona network considered

463

---

the network change according to its state, that is, it is a hybrid system. This would imply extending the proposed approach to hybrid systems. This is currently an on-going work which preliminary results can be found in Vento et al. (2010).

	f_L3	f_L7	f_L8	f_L9	f_L16	f_L19	f_L27	f_L39	f_L41	f_L45	f_L47	f_L53	f_L54	f_L56	f_L80	f_P4	f_P6	f_P13	f_P16	f_P20
r_L3	X						X										X			
r_L7		X										X							X	
r_L8			X		X															X
r_L9				X												X				
r_L16					X			X							X	X				
r_L19						X												X		
r_L27							X													X
r_L39								X											X	
r_L41								X	X										X	
r_L45									X	X	X									
r_L54												X	X	X						
r_L56														X					X	
r_L80											X				X					

Fig. 8. Boolean fault signature matrix of limnimeter: residuals are in rows and faults in columns

("X" represents "1" and a blank a "0")

6.2.2 Liminmeter interval model identification

After the structure of the model for each limnimeter has been obtained, the nominal values and intervals for the parameters are determined using the interval identification method presented in *Section 2.3*. In order to illustrate how such procedure works, the interval model identification of liminimeter L_{03} is presented. According to Figure 7, the model of this limnimeter has the following structure $L_{03}(k+1) = aL_{03}(k) + bL_{27}(k) + cP_{06}(k)$ according to Eq. (6). Thus, to use the interval identification algorithm, this model should be expressed in regressor form (8). In this case, the regressor is given by $\varphi(k) = \begin{bmatrix} L_{03}(k) & L_{27}(k) & P_{06}(k) \end{bmatrix}$ while the vector of parameters is given by $\theta(k) = \begin{bmatrix} a & b & c \end{bmatrix}^{T}$. A set of 50 selected real scenarios between 1999 and 2003, free of faults, have been selected for estimating the model parameters and their intervals. The resulting nominal values are $\theta^{o} = \begin{bmatrix} 0.9014 & 0.06717 & 0.1861 \end{bmatrix}^{T}$ while the intervals are given by $\mathbf{H} = diag(0.0451, 0.0034, 0.0093)$ according to Eq. (9). Figure 9 shows the interval model prediction using the nominal parameter values and intervals for limnimeter L_{03} for a subset of data used for estimation, while Figure 10 shows the interval model prediction for a subset of data used for validation.

20
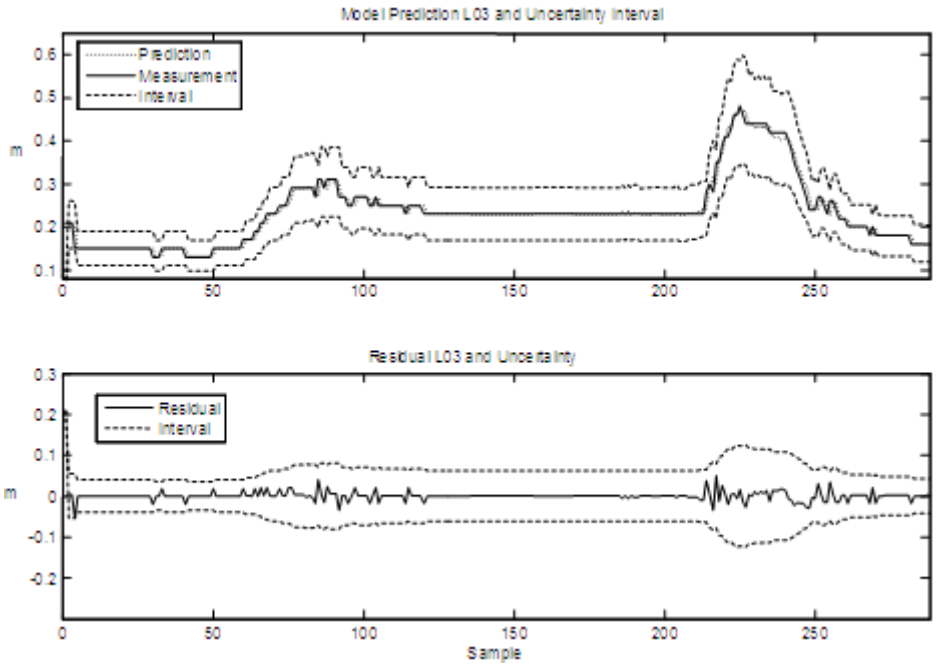
Fig. 9. Estimation of interval model corresponding to limnimeter L_{03}
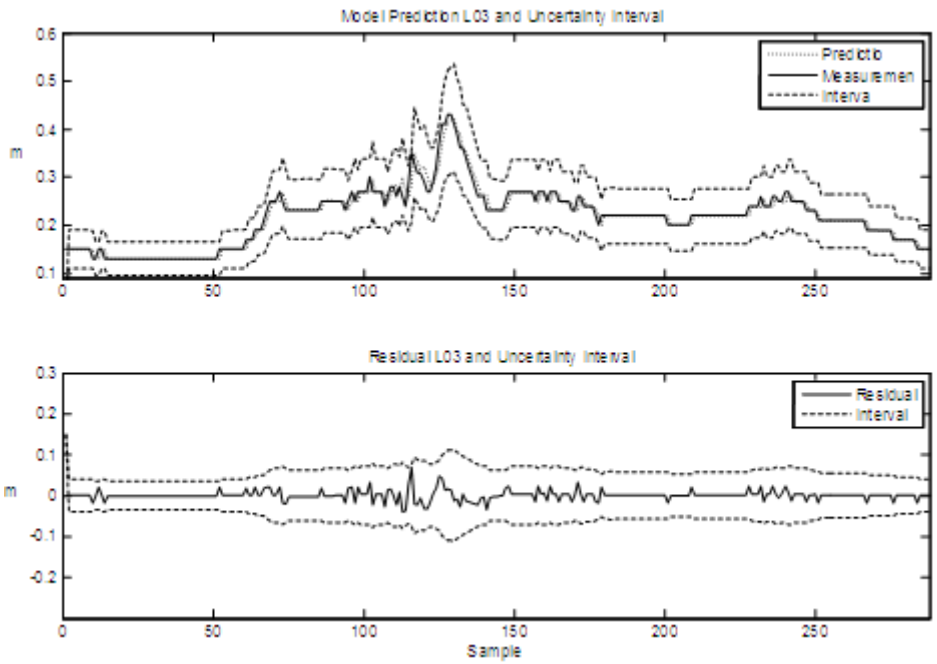

Fig. 10. Validation of interval model corresponding to limnimeter L_{03}

6.2.3 Liminimeter fault scenario

To show how the fault isolation procedure proposed in this paper works in case of liminimeters, a real fault scenario recorded at 14/09/1999 affecting L_{27} is studied. A fault in this sensor appeared at time instant *4000s*. Figure 11 presents residuals r_{03}^{0}

21

493 and $r_{27}{}^0$, that is, the residuals where L_{27} is involved according to fault signature matrix (see Figure 8). Those residuals are

494 evaluated using the adaptive threshold provided by their interval model. The fault is detected when the limnimeter

495 measurement (in continous line) goes out to the prediction interval (in dash line). Notice that the fault in both residuals is

496 detected at different time instants. Moreover, notice that residual $r_{27}{}^0$ is activated only for a short period of time, although the

497 fault is still present. The reason is because detection is based on using parity equations that use model (8) in regressor form.

498 Since the model prediction (8) uses the faulty measurements, after some samples this prediction is contaminated by the fault

499 and the residual come back inside the prediction interval. This phenomenon is known as the *fault following effect* (see Puig,

500 2008 for more details).

501 Figure 12 shows the time evolution of fault isolation factors (***factor01***, ***factorsign***, ***factorsensit***, ***factororder*** and ***factortime***).

502 The fault isolation process starts after the first residual $r_{27}{}^0$ is activated at time instant *4000 s* (see Figure 11). Using only

503 binary information (***factor01***), the fault candidates would be first L_{27} but later L_{03}, as it can be seen from Figure 12. This is due

504 to the fact that the first the residual $r_{27}{}^0$ activates, but later it is deactivated (lack of persistence in the fault signal indication). In

505 particular, when $r_{03}{}^0$, that appears later (at time *7900*s), is activated, $r_{27}{}^0$ is deactivated. So, residuals $r_{03}{}^0$ and $r_{27}{}^0$ are never

506 activated at the same time. However, using the information of ***factororder***, a fault in L_{03} would imply that the first residual

507 activated should be $r_{03}{}^0$ instead of $r_{27}{}^0$. So, L_{03} can be already excluded as a fault candidate because is not consistent with the

508 expected order of activation. Later, at time *7900*s, the second residual $r_{03}{}^0$ is activated confirming that the fault is in $L_{27.}$

509 Moreover, from the ***factortime***, the FDI module knows that the fault isolation process is ended and it has not to wait until the
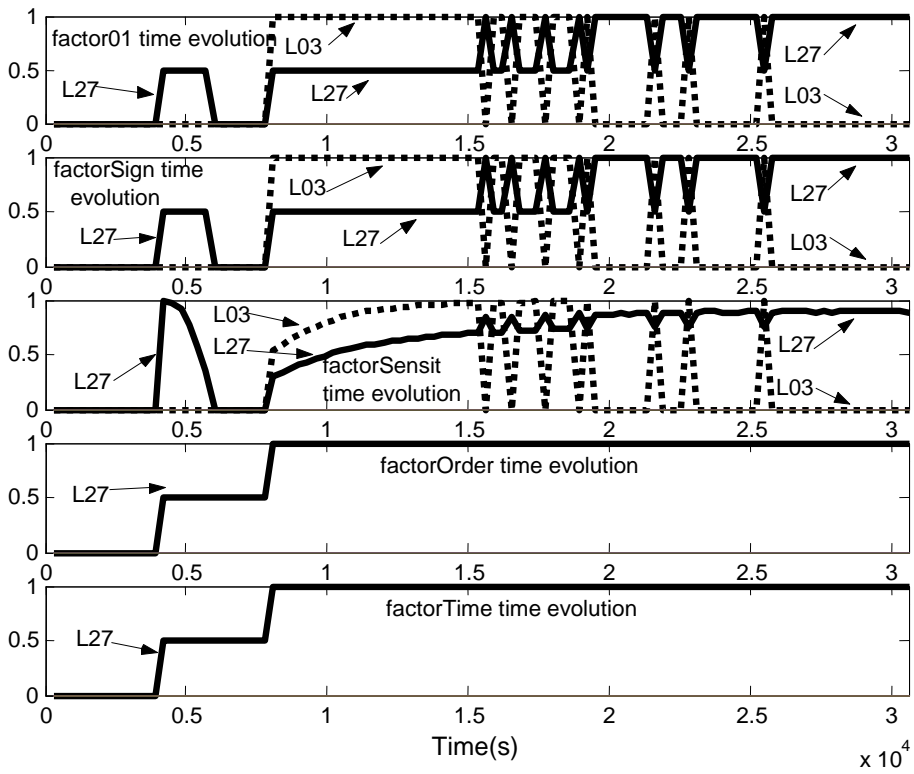
510 end of the time window.

511
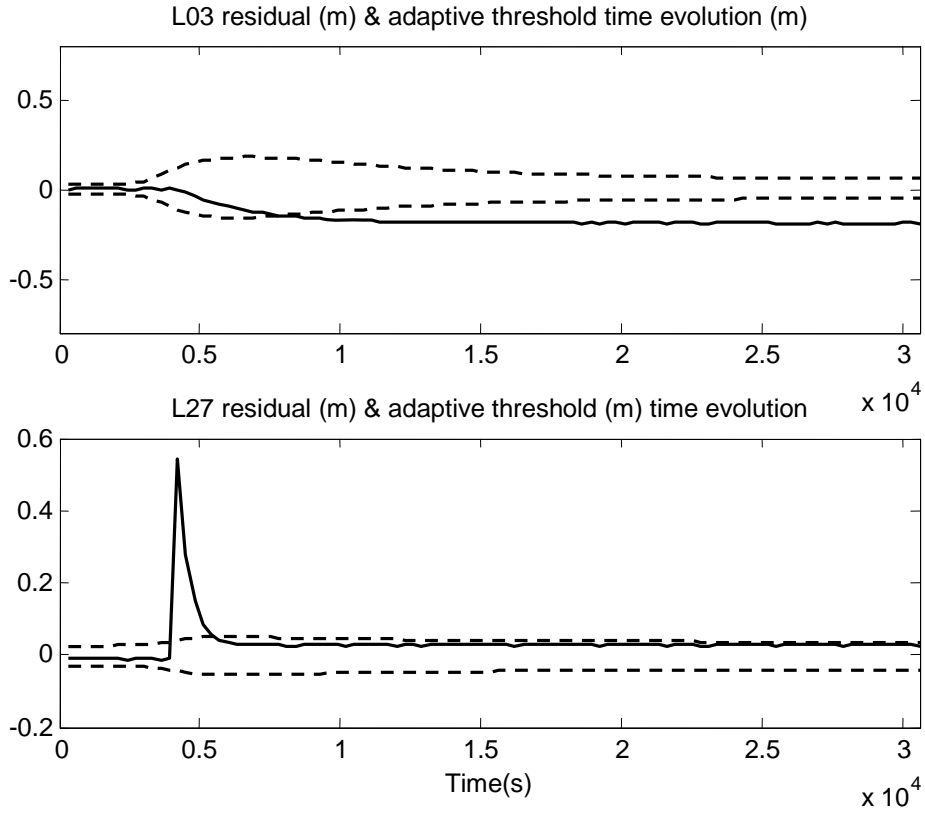
Fig. 11. Time evolution of the residuals r_{03}^0 and r_{27}^0 with their adaptive thresholds

Fig. 12. Time evolution of factor indicators

516

6.2.4 Evaluation of the FDI performance

518

Fault detection performance has been assessed by the evaluation of the minimum detectable fault defined in *Section 4.1*. The initial and steady state values of the minimum detectable fault for the different residuals are presented in *Appendix 3*. Since the proposed method stores and works with the maximum value of activated fault signals according to (20), the minimum detectable fault size is given by the maximum value of the residual fault sensitivity (see Eq. (18)).

On the other hand, regarding fault isolation performance, the minimum isolable fault corresponding to each fault can be obtained by finding the maximum of the minimum detectable faults associated to all the residuals that are sensitive to this fault. This fact implies that the minimum isolable fault in case of the proposed approach will be smaller than in the case of the standard FDI approach. The reason is related to the fact that in the proposed approach the minimum detectable fault size is given by the maximum value of the residual fault sensitivity as discussed above. This can be easily seen by looking at the results presented in *Appendix 3*. Looking for example at output faults (diagonal of the tables in Appendix 3), the smaller size of minimum detectable fault corresponds to the one obtained with the initial fault sensitivity value computed using (18) considering $S_f(q^{-1})|_{q=1}$. On the other hand, using the classic FDI approach (see Gertler, 1998) which reasons continuously with residuals using a column-based reason scheme, since all the residuals sensitive to a fault should be activated to isolate the fault, the minimum isolable fault corresponding to each fault can be obtained by finding the maximum of the minimum steady state detectable faults computed using (18) considering $S_f(q^{-1})|_{q\to\infty}$. As it can be noticed from the tables in *Appendix 3*, the values of the initial minimum detectable faults for outputs faults are smaller than the corresponding ones in steady state.

535

6.3 FDI in rain-gauges

537

6.3.1 Introduction

539

The telemetry system of Barcelona sewer network contains 22 rain gauges that are connected to the CLABSA control centre and provide the rain intensity every 5 minutes. Figure 13 presents the location of those rain-gauges on the Barcelona map. Each rain gauge is represented by a small square and a name (black squares correspond to the rain-gauges used in the test catchment presented in Fig. 7, while red squares are the rest of rain-gauges of the sewer network). Spatial models for rain-gauges are derived from the correlation analysis (based on the computation of the correlation matrix) between all the existent rain-gauges in the telemetry system. This allows deriving which are the most correlated rain-gauges with a given rain-gauge

24

546 under test. These correlation analyses have been applied not only to a particular rain scenario but to a 48 rain scenarios in a 5

547 year rain-data records. The result of the correlation analysis for the whole set of rain-gauges of the Barcelona sewer network is

548 presented in the table presented in Figure 14. In this table, for each rain-gauge in rows appear the three most correlated

549 (derived from the correlation matrix) rain-gauges with the associated explained variance.

550
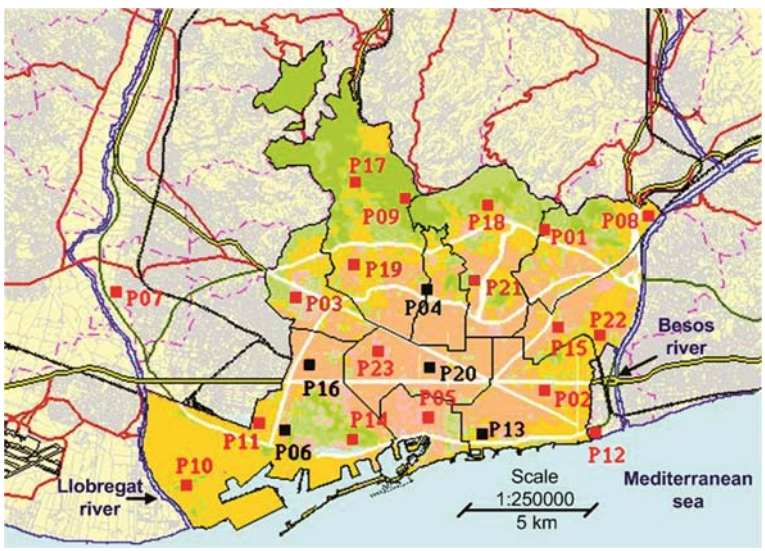
551 Fig. 13. Barcelona's rain-gauge network (rain-gauges are represented with squares)

552

	1	%	2	%	3	%
P01	18	15.60	21	12.76	8	12.76
P02	15	17.02	12	15.60	13	14.18
P03	19	26.08	16	16.66	17	7.97
P04	21	22.22	20	17.77	19	9.62
P05	20	17.24	14	14.94	13	14.94
P06	11	26.66	14	20.74	10	17.77
P07	3	14.39	10	11.36	19	11.36
P08	1	21.01	15	13.04	22	12.31
P09	17	20.13	19	15.97	18	15.97
P10	11	25.18	6	22.22	14	12.59
P11	6	28.88	10	18.51	14	14.07
P12	2	23.07	13	22.22	15	11.96
P13	2	14.89	12	13.47	5	11.34
P14	6	21.01	16	13.76	11	12.31
P15	2	18.75	22	18.05	21	12.50
P16	3	15.21	6	13.04	19	10.86
P17	9	22.91	19	19.44	3	11.80
P18	1	15.27	21	14.58	9	13.19
P19	3	23.91	17	15.21	4	11.59
P20	4	18.84	5	12.31	13	10.86
P21	4	19.14	15	13.47	18	11.34
P22	15	24.82	2	16.31	21	8.51

553

554 Fig. 14. Correlation table of the rain-gauges of Barcelona sewer network

555

556 Once the most correlated rain-gauges have been derived the following question to answer is how many rain-gauge should be

557 considered in order to build a fault detection model for a given rain-gauge. To answer this question, there is a compromise

558 between fault detection and fault isolation model properties. An increase in the number of rain-gauges used to model the rain-

25

559   gauge under test improves the model prediction quality, but decreases the capacity to isolate the faulty rain-gauge due to a

560   model is affected by the faults of more rain-gauges. In Figueras *et al*. (2005), it has been shown that three rain-gauges,

561   providing the 70% of data variance, was a good number in this application since provide the best trade-off between model

562   quality and fault isolation capabilities in case of multiple sequential faults. Figure 15 presents the fault signature matrix in case

563   that the three most correlated rain-gauges are used to build the models.

564

	f_{P1}	f_{P2}	f_{P3}	f_{P4}	f_{P5}	f_{P6}	f_{P7}	f_{P8}	f_{P9}	f_{P10}	f_{P11}	f_{P12}	f_{P13}	f_{P14}	f_{P15}	f_{P16}	f_{P17}	f_{P18}	f_{P19}	f_{P20}	f_{P21}	f_{P22}
r_{P1}	X							X										X			X	
r_{P2}		X										X	X		X							
r_{P3}			X													X	X		X			
r_{P4}				X																X	X	X
r_{P5}					X								X	X						X		
r_{P6}						X				X	X			X								
r_{P7}			X				X			X									X			
r_{P8}	X							X							X							X
r_{P9}									X								X	X	X			
r_{P10}						X				X	X			X								
r_{P11}						X				X	X			X								
r_{P12}		X										X	X		X							
r_{P13}		X			X								X	X								
r_{P14}						X					X			X		X						
r_{P15}		X													X						X	X
r_{P16}		X			X											X			X			
r_{P17}		X						X									X		X			
r_{P18}	X							X										X			X	
r_{P19}			X	X													X		X			
r_{P20}				X	X								X							X		
r_{P21}				X											X			X			X	
r_{P22}															X						X	X

565

566   Fig. 15. Boolean signature of the rain-gauge residuals (in rows) of Barcelona's network

567   and faults (in columns) ("X" represents "1" and a blank a "0")

568

569   *6.3.2 Rain-gauge interval model identification*

570   As in the case of liminimeters, once the structure of the model for each rain-gauge has been derived, the nominal values and

571   intervals for the parameters are determined using the interval identification method presented in *Section 2.3*. In order to

572   illustrate how such procedure works in this case, the interval model identification of rain-gauge P_{04} is presented. According to

573   Figure 15, the model of this rain-gauge considering the three most correlated ones has the following

574   structure: $P_{04}(k) = \alpha_1 P_{19}(k) + \alpha_2 P_{20}(k) + \alpha_3 P_{21}(k)$ (see Eq. (7)). . Thus, to use the interval identification algorithm, this model

575   should be expressed in regressor form (8) with the regressor given by $\boldsymbol{\varphi}(k) = \begin{bmatrix} P_{19}(k) & P_{20}(k) & P_{21}(k) \end{bmatrix}$ while the vector of

576 parameters is given by $\theta(k) = [\alpha_1 \quad \alpha_2 \quad \alpha_3]^T$. As in the case of liminimeters, a set of 50 scenarios between 1999 and 2003,

577 free of faults, have been selected for calibrating the model parameters and their intervals. The resulting nominal values are

578 $\theta^o = [0.1939 \quad 0.3582 \quad 0.4479]^T$ while the intervals are given by $\mathbf{H} = diag(0.0097, 0.0179, 0.0224)$ according to Eq. (9).

579 Figure 16 shows the interval model prediction for rain-gauge P_{04} for a subset of data used for estimation, while Figure 17

580 shows the interval model prediction for a subset of data used for validation.

581
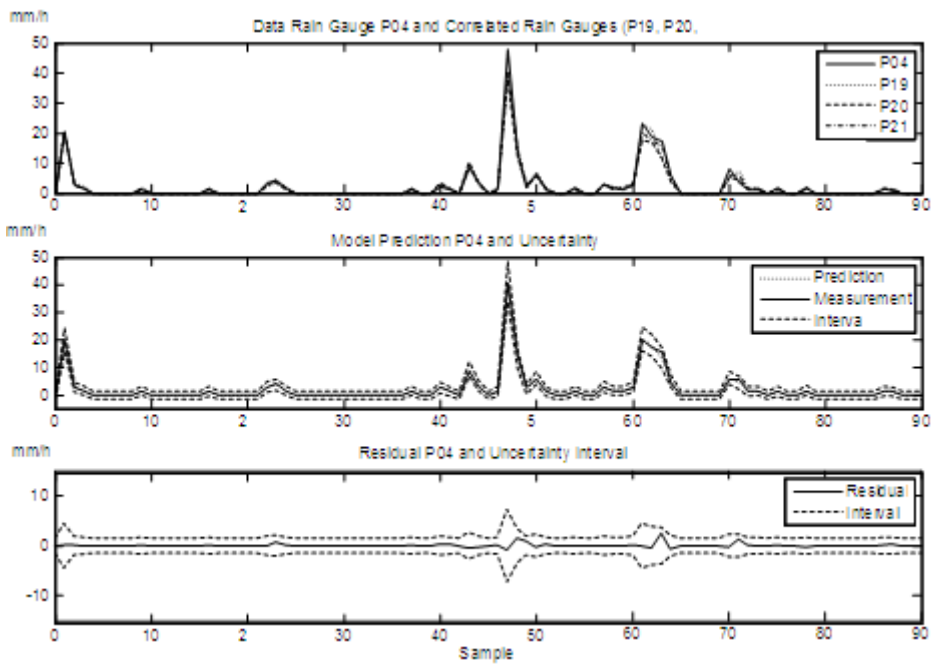
583 Fig. 16. Estimation of interval model corresponding to limnimeter P_{04}

584
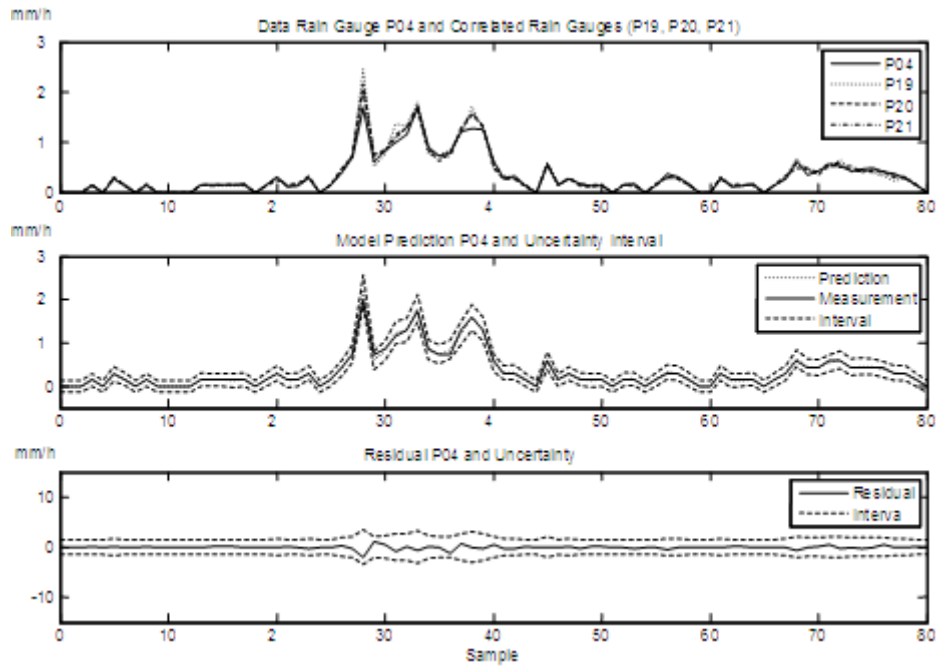
Fig. 17. Validation of interval model corresponding to limnimeter P_{04}

6.3.3 Rain-gauge faulty scenario

To show the effectiveness of the proposed FDI approach in case of rain-gauges, a real fault scenario recorded at 15/11/2001 is considered. In this case, a fault in rain-gauge P_9 was present. This fault was noticed by sewer network operators just by visual inspection comparing this rain gauges with the closest (most correlated) ones. Results from checking real measurements taken from rain-gauge P_9 are compared with their corresponding prediction interval generated using an interval model built from the three most correlated rain-gauges (P_{17}, P_{18} and P_{19}) (see Figure 18). Figure 19 and 20 presents the residuals corresponding to rain-gauges P_{17} and P_{18} where rain-gauge P_9 is also used according to the fault signature matrix in Figure 15. Figure 21 presents the time evolution of *factorsensit* for the rain-gauges P_9, P_{17} and P_{18}. It can be noticed that P_9 will be proposed as the candidate faulty rain-gauge according to (21). Since rain-gauge models are static, *factortime* and *factororder* are not used in the rain-gauge fault isolation.

28

599
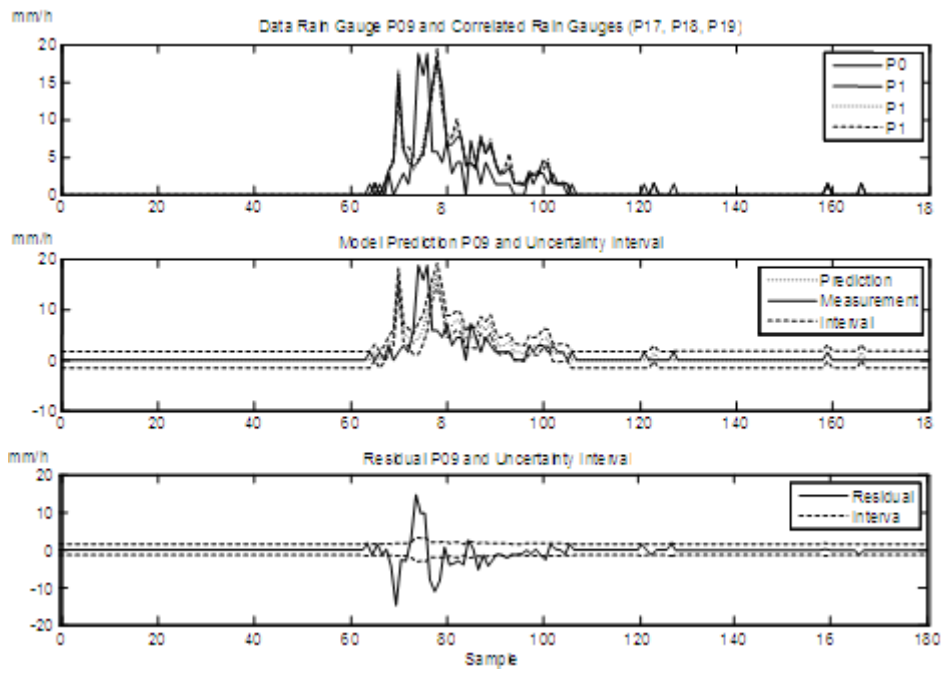
600   Fig. 18 Fault in rain-gauge P_{09} in the 15/11/2001 rain-scenario

601

602
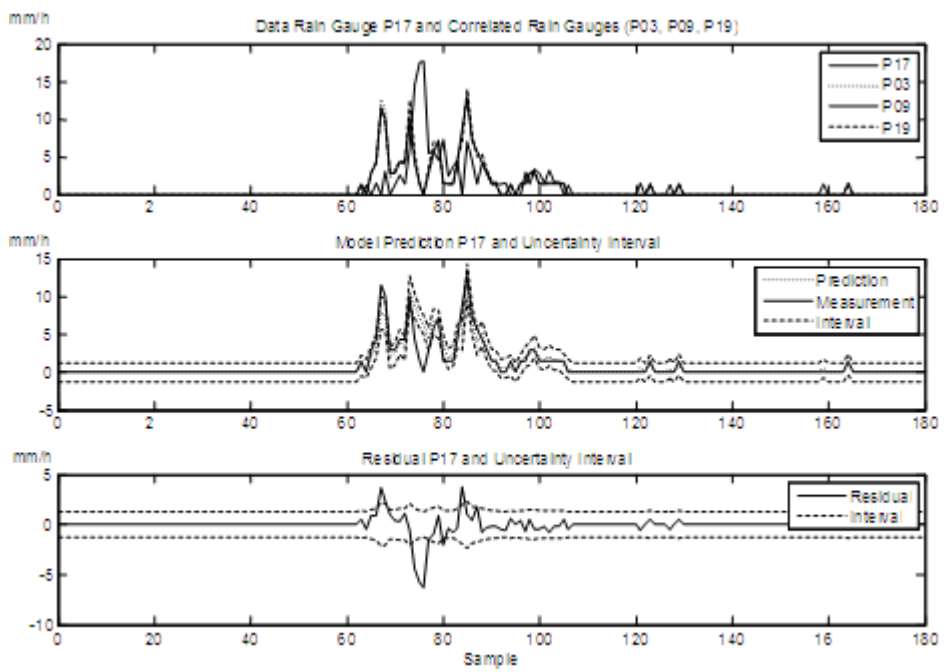
603   Fig. 19. Fault in rain-gauge P_{09} in the 15/11/2001 rain-scenario

604

605
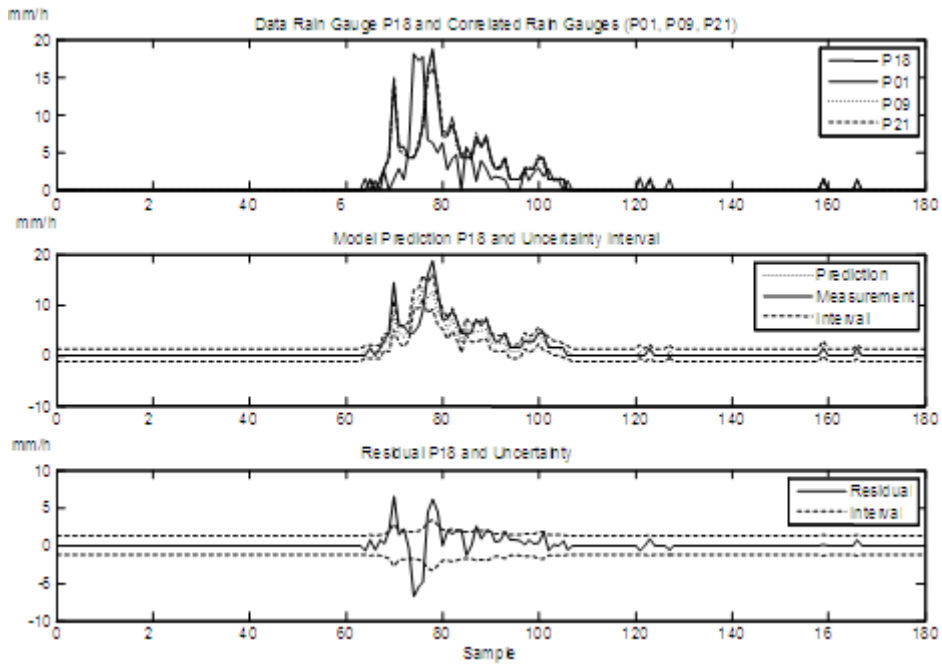
606   Fig. 20. Fault in rain-gauge P_{09} in the 15/11/2001 rain-scenario

607
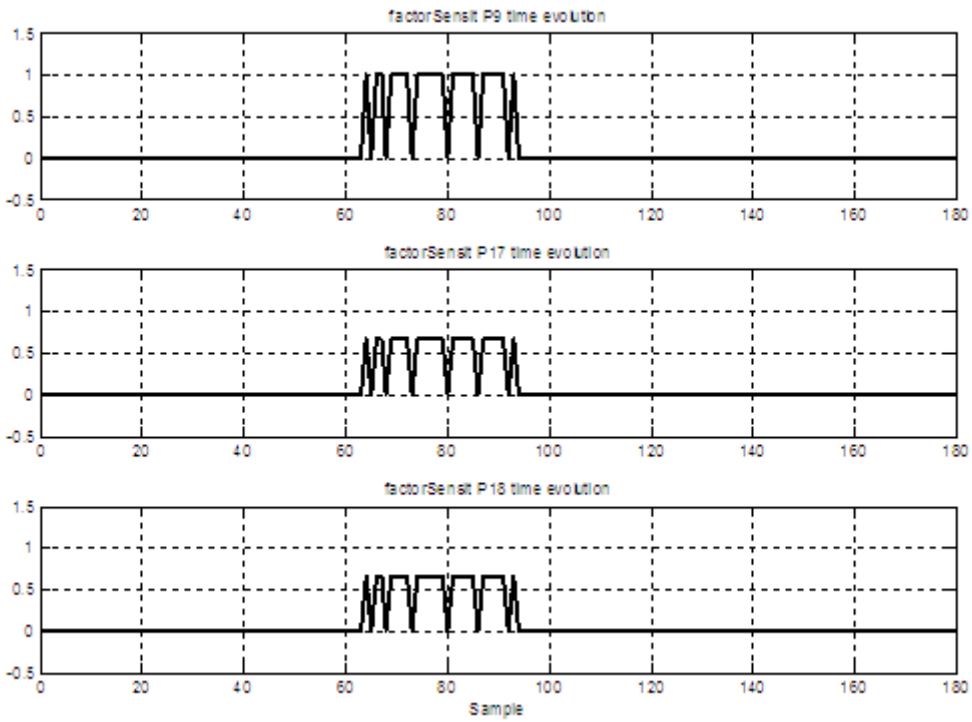
608   Fig. 21. Time evolution of *factorsensit* indicators

609

610

611

612

7. CONCLUSIONS

In this paper, fault detection and isolation in rain gauges and limnimeters of Barcelona's urban sewer system is presented. The proposed FDI strategy is based on building a linear interval model for every instrument. Then, each instrument is tested according the prediction provided by its interval model obtained from real data using the parity equation approach. While, the real measurement is inside the interval of predicted behaviour no fault can be indicated. However, when the measurement is outside its envelope a fault can be indicated. Once the fault has been detected, a fault isolation procedure is initiated in order to isolate the faulty instrument. Fault isolation is based on matching of the fault signature with a set of theoretical fault signatures. Finally, the proposed FDI system is applied to several real scenarios providing promising results in order to be applied in real-time operation. As a further work the proposed method will be applied to faults in actuators. Currently, the proposed FDI method is being integrated with MPC control system of the sewer network in order to validate rain-gauges and limnimeters readings. In case that some instrument is in faulty situation, some fault tolerance mechanism should be activated to allow the control system to continue in operation. The design of these fault tolerance mechanisms are also currently under development.

APPENDIX 1

This appendix describes the different fault signatures matrices used for the fault isolation module presented in *Section 5* as well as their usage:

FSM01: Evaluation of fault signal appearance. The ***FSM***01-table contains the theoretical binary patterns that faults produce in the residual equations. Those patterns can be codified using the values 0 for no influence, 1 otherwise. ***factor01***$_j$ is calculated for the jth fault hypothesis in the following way:

$$\boldsymbol{factor}01_j = \frac{\sum\limits_{i=1}^{n}\left(boolean\left(\phi_{i,\max}\right)\boldsymbol{FSM}01_{ij}\right)}{\sum\limits_{i=1}^{n}\boldsymbol{FSM}01_{ij}}\boldsymbol{zvf}_j \tag{22}$$

with

$$boolean(\phi_{i,\max}) = \begin{cases} 0, & \text{if } \phi_{i,\max} = 0 \\ 1, & \text{if } \phi_{i,\max} \neq 0 \end{cases}$$

and the zero-violation-factor as

639
$$zvf_j = \begin{cases} 0, & \text{if } \exists \ i \in \{1,...,n\} \ \text{ with } \ \boldsymbol{FSM01}_{ij} = 0 \\ & \qquad\qquad\quad \text{and } \ \phi_{i,\max} \neq 0 \\ 1, & \text{otherwise} \end{cases}$$

640 This leads to the following behaviour: expected fault signals support a fault hypothesis, unexpected fault signals are eliminated

641 through the zero-violation-factor. Missing fault signals influence the supportability of a hypothesis indirectly via the

642 denominator of Eq. (22).

643

644 *FSMsign:* Evaluation of fault signal signs. The *FSMsign*-table contains the theoretical sign patterns that faults produce in the

645 residual equations. Those patterns can be codified using the values 0 for no influence, +1/-1 for positive/negative deviation for

646 every $\boldsymbol{FSMsign}_{ij}$.

647

648 The $\boldsymbol{factorsign}_j$ is calculated comparing theoretical signs to the signs stored in the memory:

649

650
$$\boldsymbol{factorsign}_j = \frac{\boldsymbol{numsign}_j}{\sum\limits_{i=1}^{n} \left| \boldsymbol{FSMsign}_{ij} \right|} \boldsymbol{zvfsign}_j \tag{23}$$

651 where the number of signs in the fault signal vector that coincides with each jth fault hypothesis, considering either the case

652 that all residuals have been violated in the positive or negative patterns in $\boldsymbol{FSMsign}_{ij}$ is given by

653

654
$$\begin{aligned} numsign_j = \max(&\sum_{i=1}^{n} ckecksign(\phi_{i,\max}, \boldsymbol{FSMsign}_{ij}), \\ &\sum_{i=1}^{n} ckecksign(\phi_{i,\max}, -\boldsymbol{FSMsign}_{ij})) \end{aligned}$$

655 with

656
$$\begin{aligned} ckecksign(&\phi_{i,\max}, \boldsymbol{FSMsign}_{ij}) = \\ &\begin{cases} 0 & sign(\phi_{i,\max}) \neq sign(\boldsymbol{FSMsign}_{ij}) \\ 1 & sign(\phi_{i,\max}) = sign(\boldsymbol{FSMsign}_{ij}) \end{cases} \end{aligned}$$

657

658 where the factor $zvfsign_j$ is defined in a similar way as in the case of $\boldsymbol{factor}01$, excluding those fault hypothesis that has a

659 zero in a position where the fault signal presents a sign. The *sign* function is defined as in MATLAB, i.e., $sign(x) = 1$ if $x > 0$,

660 $sign(x) = -1$ if $x < 0$ and $sign(x) = 0$ if $x = 0$.

661

32

662   **FSM***sensit:* Evaluation of fault sensitivities. This evaluation component uses the fault signal activation values $\phi_{i,\max}$ from the

663   memory table and computes **factor***sensit* using the sensitivity-based **FSM***sensit* table for weighting the activation values. That

664   approach can be found as well in the DMP-method (Petti, *et al.,* 1990). The following equations describe how to calculate the

665   entries **FSM***sensit*$_{ji}$

666

667    $$\textbf{FSM}sensit_{ij} = \begin{cases} \dfrac{S_{ij}}{\left|\overline{r_i^o(k))}\right|} & if \quad r_i^o(k) \geq 0 \\[4mm] \dfrac{S_{ij}}{\left|(\underline{r}_i^o(k)\right|} & if \quad r_i^o(k) < 0 \end{cases} \tag{24}$$

668   with the sensitivity defined as $S_{ij} = \dfrac{\partial r_i^o}{\partial f_j}$. Although, the sensitivity depends on time in case of a dynamic system, here the

669   steady-state value after a fault occurrence is considered as it was also suggested in (Gertler, 1998). The value of **FSM***sensit*$_{ij}$

670   describes, how easily a fault will cause a violation of the threshold of the ith residual since the larger its partial derivative with

671   respect to the fault, the more sensitive that equation is to deviations of the assumption. Similarly, residuals with large detection

672   thresholds are less sensitive as they are more difficult to violate. Therefore **FSM***sensit*$_{ij}$ can be used to weight the activation

673   value of different fault signals:

674

675    $$\textbf{factor}sensit_j = \frac{\sum_{i=1}^{n}\left(\phi_{i,\max}\textbf{FSM}sensit_{ij}\right)}{\sum_{i=1}^{n}\left|\textbf{FSM}sensit_{ij}\right|} zvfsensit_{ij} \tag{25}$$

676

677   where the factor $zvfsensit_j$ is defined in a similar way as in the case of **factor**01, excluding those fault hypothesis that has a

678   zero theoretical sensitivity while fault signal presents an non-zero value.

679

680   **FSM***order:* Evaluation of fault signal appearance order. In dynamic systems a fault f_j does not affect at same time all

681   residuals. **FSM***order* table contains the order of the fault signal apparition for each fault hypothesis; this order is codified

682   using ordinal numbers, starting with '1'. If two fault signals appear at the same time, then they should share the same ordinal

683   number. Fault signals that are not associated to an fault hypothesis get the code '0' (Meseguer, 2007;2009). The **factor***order* is

684   calculated comparing the apparition order of the fault signal to the theoretical order stored in the memory. This comparison

33

685   requires to count the number of apparition order coincidences between the fault signal vector and each jth fault hypothesis

686   according to:

687
$$factororder_j = \frac{\sum_{i=1}^{n}\left(order\left(\phi_{i,\max},\textbf{FSMorder}_{ij}\right)\right)}{\sum_{i=1}^{n}boolean(\textbf{FSMorder}_{ij})} zvforder_{ij} \tag{26}$$

688   where

689
$$order(\phi_{i,\max},\textbf{FSMorder}_{ij}) =$$
$$\begin{cases} 0 & order(\phi_{i,\max}) \neq \textbf{FSMorder}_{ij} \\ 1 & order(\phi_{i,\max}) = \textbf{FSMorder}_{ij} \end{cases}$$

690

691   and $order(\phi_{i,\max})$ is the order of apparition in which the ith fault signal has activated with respect to the first activated. Such

692   order is recorded in the memory component. The factor $zvforder_j$ is defined in a similar way as in the case of $\textbf{\textit{factor}}01$,

693   excluding those fault hypothesis that do not coincides in the order .

694

695   <u>$\textbf{\textit{FSMtime}}$</u>: Evaluation of fault signal appearance time. The element $\textbf{FSMtime}_{ij}$ of matrix $\textbf{FSMtime}$ contains the time interval

696   $[\underline{\tau}_{ij},\overline{\tau}_{ij}]$ in which the fault signal ϕ_i caused by fault f_j is expected to appear. This time interval is referred to the occurrence

697   time instant of the first fault signal according to the fault hypothesis f_j as in most of the cases, the fault occurrence time instant

698   t_0 is unknown. (Meseguer et al., 2007) shows that the interval $[\underline{\tau}_{ij},\overline{\tau}_{ij}]$ basically depends on the sensitivity of the residual

699   $r_i^o(k)$ to fault f_j ($S_{f_{ij}}$), on the adaptive threshold $[\underline{r}_i^o(k),\overline{r}_i^o(k)]$ associated to this residual and on t_0. Thus, the elements of

700   matrix $\textbf{FSMtime}$ are given by

701
$$\textbf{FSMtime}_{ij} = \begin{cases} [\underline{\tau}_{ij},\overline{\tau}_{ij}] & if \quad S_{f_{ij}} \neq 0 \\ [-1,-1] & if \quad S_{f_{ij}} = 0 \end{cases} \tag{27}$$

702

703   From $\textbf{FSMtime}$ matrix, the time window T_w which determines the maximum period of time required once the first fault signal

704   is observed so that all fault signals can appear can be determined as follows

705
$$T_w = \max_{\forall i,j}(\overline{\tau}_{ij}) \tag{28}$$

706   On the other hand, in order to compare the occurrence time instant of the observed fault signal sequence with the stored one in

707   matrix $\textbf{FSMtime}$, the factor $\textbf{\textit{factortime}}_j$ is calculated for every fault hypothesis as it follows:

708

34

709

$$factortime_j(k) = \frac{\sum_{i=1}^{ny}\left(ckecktime\left(k_{\phi i}, k_{ref}, \boldsymbol{FSMtime}_{ij}\right)\right)}{\sum_{i=1}^{ny} boolean(\boldsymbol{FSMtime}_{ij})} zvf_j \qquad (29)$$

710 where $k_{\phi i}$ is the apparition time instant of the fault signal $\phi_i(k)$, k_{ref} is the apparition time instant of the first observed fault

711 signal,

$$ckecktime\left(k_{\phi i}, k_{ref}, \boldsymbol{FSMtime}_{ij}\right) =$$

712
$$\begin{cases} 0 & if \quad k_{\phi i} - k_{ref} \notin \boldsymbol{FSMtime}_{ij} \text{ or } |\phi_i(k)| < 0.5 \\ 1 & if \quad k_{\phi i} - k_{ref} \in \boldsymbol{FSMtime}_{ij} \text{ and } |\phi_i(k)| \geq 0.5 \end{cases} \qquad (30)$$

713

714
$$boolean(\boldsymbol{FSMtime}_{ij}) = \begin{cases} 0, & \text{if } \boldsymbol{FSMtime}_{ij} = [-1,-1] \\ 1, & \text{if } \boldsymbol{FSMtime}_{ij} \neq [-1,-1] \end{cases} \qquad (31)$$

715 and where zvf_j is the zero-violation-factor whose expression is

716
$$zvf_j = \begin{cases} 0, & \text{if } \exists \ i \in \{1,...,n\} \text{ with } \boldsymbol{FSM}01_{ij} = 0 \\ & \qquad\qquad\qquad \text{and } |\phi_i(k)| \geq 0.5 \\ 1, & \text{otherwise} \end{cases} \qquad (32)$$

717

718

719   APPENDIX 2

720 This appendix presents the contents of the different fault signatures matrices used for the fault isolation module of limnimeters

721 in the Barcelona sewer network case study.

722
723

FSM01 Matrix

	f_{L3}	f_{L7}	f_{L8}	f_{L9}	f_{L16}	f_{L19}	f_{L27}	f_{L39}	f_{L41}	f_{L45}	f_{L47}	f_{L53}	f_{L54}	f_{L56}	f_{L80}
ϕ_{L3}	1	0	0	0	0	0	1	0	0	0	0	0	0	0	0
ϕ_{L7}	0	1	0	0	0	0	0	0	0	0	0	1	0	0	0
ϕ_{L8}	0	0	1	0	1	0	0	0	0	0	0	0	0	0	0
ϕ_{L9}	0	0	0	1	0	0	0	0	0	0	0	0	0	0	0
ϕ_{L16}	0	0	0	0	1	0	0	0	0	0	0	0	0	0	1
ϕ_{L19}	0	0	0	0	0	1	0	0	0	0	0	0	0	0	0
ϕ_{L27}	0	0	0	0	0	0	1	0	0	0	0	0	0	0	0
ϕ_{L39}	0	0	0	0	0	0	0	1	0	0	0	0	0	0	0
ϕ_{L41}	0	0	0	0	0	0	0	1	1	0	0	0	0	0	0
ϕ_{L45}	0	0	0	0	0	0	0	0	1	1	1	0	0	0	0
ϕ_{L54}	0	0	0	0	0	0	0	0	0	0	0	0	1	1	1	0
ϕ_{L56}	0	0	0	0	0	0	0	0	0	0	0	0	0	1	0
ϕ_{L80}	0	0	0	0	0	0	0	0	0	0	1	0	0	0	1

724
725

FSM sign Matrix

	f_{L3}	f_{L7}	f_{L8}	f_{L9}	f_{L16}	f_{L19}	f_{L27}	f_{L39}	f_{L41}	f_{L45}	f_{L47}	f_{L53}	f_{L54}	f_{L56}	f_{L80}
ϕ_{L3}	+1	0	0	0	0	0	-1	0	0	0	0	0	0	0	0
ϕ_{L7}	0	+1	0	0	0	0	0	0	0	0	0	-1	0	0	0
ϕ_{L8}	0	0	+1	0	-1	0	0	0	0	0	0	0	0	0	0
ϕ_{L9}	0	0	0	+1	0	0	0	0	0	0	0	0	0	0	0
ϕ_{L16}	0	0	0	0	+1	0	0	0	0	0	0	0	0	0	-1
ϕ_{L19}	0	0	0	0	0	+1	0	0	0	0	0	0	0	0	0

ϕ	f_{L3}	f_{L7}	f_{L8}	f_{L9}	f_{L16}	f_{L19}	f_{L27}	f_{L39}	f_{L41}	f_{L45}	f_{L47}	f_{L53}	f_{L54}	f_{L56}	f_{L80}
ϕ_{L27}	0	0	0	0	0	0	+1	0	0	0	0	0	0	0	0
ϕ_{L39}	0	0	0	0	0	0	0	+1	0	0	0	0	0	0	0
ϕ_{L41}	0	0	0	0	0	0	-1	+1	0	0	0	0	0	0	0
ϕ_{L45}	0	0	0	0	0	0	0	-1	+1	-1	0	0	0	0	0
ϕ_{L54}	0	0	0	0	0	0	0	0	0	0	-1	+1	-1	0	0
ϕ_{L56}	0	0	0	0	0	0	0	0	0	0	0	0	0	+1	0
ϕ_{L80}	0	0	0	0	0	0	0	0	0	0	-1	0	0	0	+1

726

727

728

FSM *sensit* Matrix

	f_{L3}	f_{L7}	f_{L8}	f_{L9}	f_{L16}	f_{L19}	f_{L27}	f_{L39}	f_{L41}	f_{L45}	f_{L47}	f_{L53}	f_{L54}	f_{L56}	f_{L80}
ϕ_{L3}	0.241	0	0	0	0	0	-0.156	0	0	0	0	0	0	0	0
ϕ_{L7}	0	0.115	0	0	0	0	0	0	0	0	0	-0.033	0	0	0
ϕ_{L8}	0	0	0.360	0	-0.193	0	0	0	0	0	0	0	0	0	0
ϕ_{L9}	0	0	0	0.128	0	0	0	0	0	0	0	0	0	0	0
ϕ_{L16}	0	0	0	0	0.383	0	0	0	0	0	0	0	0	0	-1
ϕ_{L19}	0	0	0	0	0	0.033	0	0	0	0	0	0	0	0	0
ϕ_{L27}	0	0	0	0	0	0	0.082	0	0	0	0	0	0	0	0
ϕ_{L39}	0	0	0	0	0	0	0	0.379	0	0	0	0	0	0	0
ϕ_{L41}	0	0	0	0	0	0	0	-0.958	0.042	0	0	0	0	0	0
ϕ_{L45}	0	0	0	0	0	0	0	0	-0.254	0.014	0.187	0	0	0	0
ϕ_{L54}	0	0	0	0	0	0	0	0	0	0	0	-0.810	1	-0.393	0
ϕ_{L56}	0	0	0	0	0	0	0	0	0	0	0	0	0	0.080	0
ϕ_{L80}	0	0	0	0	0	0	0	0	0	0	-0.580	0	0	0	0.256

729
730

FSM *order* Matrix

	f_{L3}	f_{L7}	f_{L8}	f_{L9}	f_{L16}	f_{L19}	f_{L27}	f_{L39}	f_{L41}	f_{L45}	f_{L47}	f_{L53}	f_{L54}	f_{L56}	f_{L80}
ϕ_{L3}	1	0	0	0	0	0	2	0	0	0	0	0	0	0	0
ϕ_{L7}	0	1	0	0	0	0	0	0	0	0	0	2	0	0	0
ϕ_{L8}	0	0	1	0	2	0	0	0	0	0	0	0	0	0	0
ϕ_{L9}	0	0	0	1	0	0	0	0	0	0	0	0	0	0	0
ϕ_{L16}	0	0	0	0	1	0	0	0	0	0	0	0	0	0	2
ϕ_{L19}	0	0	0	0	0	1	0	0	0	0	0	0	0	0	0
ϕ_{L27}	0	0	0	0	0	0	1	0	0	0	0	0	0	0	0
ϕ_{L39}	0	0	0	0	0	0	0	1	0	0	0	0	0	0	0
ϕ_{L41}	0	0	0	0	0	0	0	2	1	0	0	0	0	0	0
ϕ_{L45}	0	0	0	0	0	0	0	0	2	1	2	0	0	0	0
ϕ_{L54}	0	0	0	0	0	0	0	0	0	0	0	1	1	1	0
ϕ_{L56}	0	0	0	0	0	0	0	0	0	0	0	0	0	1	0
ϕ_{L80}	0	0	0	0	0	0	0	0	0	0	1	0	0	0	1

731

732

FSM*time* Matrix

	f_{L3}	f_{L7}	f_{L8}	f_{L9}	f_{L16}	f_{L19}	f_{L27}	f_{L39}	f_{L41}	f_{L45}	f_{L47}	f_{L53}	f_{L54}	f_{L56}	f_{L80}
ϕ_{L3}	[0,0]	[-1,-1]	[-1,-1]	[-1,-1]	[-1,-1]	[-1,-1]	[900,6300]	[-1,-1]	[-1,-1]	[-1,-1]	[-1,-1]	[-1,-1]	[-1,-1]	[-1,-1]	[-1,-1]
ϕ_{L7}	[-1,-1]	[0,0]	[-1,-1]	[-1,-1]	[-1,-1]	[-1,-1]	[-1,-1]	[-1,-1]	[-1,-1]	[-1,-1]	[-1,-1]	[2100,5400]	[-1,-1]	[-1,-1]	[-1,-1]
ϕ_{L8}	[-1,-1]	[-1,-1]	[0,0]	[-1,-1]	[600,4200]	[-1,-1]	[-1,-1]	[-1,-1]	[-1,-1]	[-1,-1]	[-1,-1]	[-1,-1]	[-1,-1]	[-1,-1]	[-1,-1]
ϕ_{L9}	[-1,-1]	[-1,-1]	[-1,-1]	[0,0]	[-1,-1]	[-1,-1]	[-1,-1]	[-1,-1]	[-1,-1]	[-1,-1]	[-1,-1]	[-1,-1]	[-1,-1]	[-1,-1]	[-1,-1]
ϕ_{L16}	[-1,-1]	[-1,-1]	[-1,-1]	[-1,-1]	[0,0]	[-1,-1]	[-1,-1]	[-1,-1]	[-1,-1]	[-1,-1]	[-1,-1]	[-1,-1]	[-1,-1]	[-1,-1]	[300,2400]
ϕ_{L19}	[-1,-1]	[-1,-1]	[-1,-1]	[-1,-1]	[-1,-1]	[0,0]	[-1,-1]	[-1,-1]	[-1,-1]	[-1,-1]	[-1,-1]	[-1,-1]	[-1,-1]	[-1,-1]	[-1,-1]
ϕ_{L27}	[-1,-1]	[-1,-1]	[-1,-1]	[-1,-1]	[-1,-1]	[-1,-1]	[0,0]	[-1,-1]	[-1,-1]	[-1,-1]	[-1,-1]	[-1,-1]	[-1,-1]	[-1,-1]	[-1,-1]
ϕ_{L39}	[-1,-1]	[-1,-1]	[-1,-1]	[-1,-1]	[-1,-1]	[-1,-1]	[-1,-1]	[0,0]	[-1,-1]	[-1,-1]	[-1,-1]	[-1,-1]	[-1,-1]	[-1,-1]	[-1,-1]
ϕ_{L41}	[-1,-1]	[-1,-1]	[-1,-1]	[-1,-1]	[-1,-1]	[-1,-1]	[-1,-1]	[300,3900]	[0,0]	[-1,-1]	[-1,-1]	[-1,-1]	[-1,-1]	[-1,-1]	[-1,-1]
ϕ_{L45}	[-1,-1]	[-1,-1]	[-1,-1]	[-1,-1]	[-1,-1]	[-1,-1]	[-1,-1]	[-1,-1]	[300,1800]	[0,0]	[300,30600]	[-1,-1]	[-1,-1]	[-1,-1]	[-1,-1]
ϕ_{L54}	[-1,-1]	[-1,-1]	[-1,-1]	[-1,-1]	[-1,-1]	[-1,-1]	[-1,-1]	[-1,-1]	[-1,-1]	[-1,-1]	[-1,-1]	[0,0]	[0,0]	[0,0]	[-1,-1]
ϕ_{L56}	[-1,-1]	[-1,-1]	[-1,-1]	[-1,-1]	[-1,-1]	[-1,-1]	[0,0]	[-1,-1]	[-1,-1]	[-1,-1]	[-1,-1]	[-1,-1]	[-1,-1]	[0,0]	[-1,-1]
ϕ_{L80}	[-1,-1]	[-1,-1]	[-1,-1]	[-1,-1]	[-1,-1]	[-1,-1]	[0,0]	[-1,-1]	[-1,-1]	[-1,-1]	[0,0]	[-1,-1]	[-1,-1]	[-1,-1]	[0,0]

733

734

APPENDIX 3

36

This appendix presents the averages values of the minimum initial and steady state detectable faults. The intervals correspond to the evaluation of Eq (18) with $\min\left(\left\|\boldsymbol{\varphi}(k)\mathbf{H}\right\|_1\right)$ and $\max\left(\left\|\boldsymbol{\varphi}(k)\mathbf{H}\right\|_1\right)$.

Initial minimum detectable faults

$\left|f_f^{\min}\right|$ with $\left.S_f(q^{-1})\right|_{q\to\infty}$

	f_{L3}	f_{L7}	f_{L8}	f_{L9}	f_{L16}	f_{L19}	f_{L27}	f_{L39}	f_{L41}	f_{L45}	f_{L47}	f_{L53}	f_{L54}	f_{L56}	f_{L80}
R_{L3}	[0.1,0.22]	∞	∞	∞	∞	∞	[0.45,1]	∞	∞	∞	∞	∞	∞	∞	∞
R_{L7}	∞	[0.06,0.1]	∞	∞	∞	∞	∞	∞	∞	∞	∞	[0.3,0.5]	∞	∞	∞
R_{L8}	∞	∞	[0.1,0.15]	∞	[0.4,0.6]	∞	∞	∞	∞	∞	∞	∞	∞	∞	∞
R_{L9}	∞	∞	∞	[0.1,0.43]	∞	∞	∞	∞	∞	∞	∞	∞	∞	∞	∞
R_{L16}	∞	∞	∞	∞	[0.1,0.35]	∞	∞	∞	∞	∞	∞	∞	∞	∞	[0.28,1]
R_{L19}	∞	∞	∞	∞	∞	[0.1,0.13]	∞	∞	∞	∞	∞	∞	∞	∞	∞
R_{L27}	∞	∞	∞	∞	∞	∞	[0.1,0.27]	∞	∞	∞	∞	∞	∞	∞	∞
R_{L39}	∞	∞	∞	∞	∞	∞	∞	[0.1,0.57]	∞	∞	∞	∞	∞	∞	∞
R_{L41}	∞	∞	∞	∞	∞	∞	∞	[0.4,1.2]	[0.1,0.32]	∞	∞	∞	∞	∞	∞
R_{L45}	∞	∞	∞	∞	∞	∞	∞	∞	[0.07,0.7]	[0.1,0.92]	[0.11,0.97]	∞	∞	∞	∞
R_{L54}	∞	∞	∞	∞	∞	∞	∞	∞	∞	∞	∞	[0.35,0.55]	[0.1,0.16]	[0.42,0.67]	∞
R_{L56}	∞	∞	∞	∞	∞	∞	∞	∞	∞	∞	∞	∞	∞	[0.1,0.39]	∞
R_{L80}	∞	∞	∞	∞	∞	∞	∞	∞	∞	[0.13,0.46]	∞	∞	∞	∞	[0.1,0.36]

Steady state minimum detectable faults

$\left|f_f^{\min}\right|$ with $\left.S_f(q^{-1})\right|_{q=1}$

	f_{L3}	f_{L7}	f_{L8}	f_{L9}	f_{L16}	f_{L19}	f_{L27}	f_{L39}	f_{L41}	f_{L45}	f_{L47}	f_{L53}	f_{L54}	f_{L56}	f_{L80}
R_{L3}	[0.4,0.91]	∞	∞	∞	∞	∞	[0.45,1]	∞	∞	∞	∞	∞	∞	∞	∞
R_{L7}	∞	[0.31,0.5]	∞	∞	∞	∞	∞	∞	∞	∞	∞	[0.3,0.5]	∞	∞	∞
R_{L8}	∞	∞	[0.3,0.45]	∞	[0.41,0.6]	∞	∞	∞	∞	∞	∞	∞	∞	∞	∞
R_{L9}	∞	∞	∞	[0.67,2.9]	∞	∞	∞	∞	∞	∞	∞	∞	∞	∞	∞
R_{L16}	∞	∞	∞	∞	[0.3,1]	∞	∞	∞	∞	∞	∞	∞	∞	∞	[0.28,1]
R_{L19}	∞	∞	∞	∞	∞	[3,30]	∞	∞	∞	∞	∞	∞	∞	∞	∞
R_{L27}	∞	∞	∞	∞	∞	∞	[0.8,2]	∞	∞	∞	∞	∞	∞	∞	∞
R_{L39}	∞	∞	∞	∞	∞	∞	∞	[0.4,2.3]	∞	∞	∞	∞	∞	∞	∞
R_{L41}	∞	∞	∞	∞	∞	∞	∞	[0.4,1.2]	[0.6,2.1]	∞	∞	∞	∞	∞	∞
R_{L45}	∞	∞	∞	∞	∞	∞	∞	∞	[0.07,0.7]	[1.1,9.2]	[0.11,0.97]	∞	∞	∞	∞
R_{L54}	∞	∞	∞	∞	∞	∞	∞	∞	∞	∞	∞	[0.35,0.55]	[0.45,0.73]	[0.42,0.67]	∞
R_{L56}	∞	∞	∞	∞	∞	∞	∞	∞	∞	∞	∞	∞	∞	[2,7.8]	∞
R_{L80}	∞	∞	∞	∞	∞	∞	∞	∞	∞	[0.13,0.46]	∞	∞	∞	∞	[0.45,1.64]

ACKNOWLEDGMENTS

754

REFERENCES

756

757 Basseville, M., Nikiforov, I. "Detection of Abrupt Changes: Theory and Applications". Prentice Hall. 2003.

758 J. Blesa, V. Puig, J. Saludes. Identification for passive robust fault detection using zonotope-based set-membership approaches.
759   *International Journal of Adaptive Control and Signal Processing*. 25 (9) 788–812. 2011.

760 Boukhris, A., Giuliani, S., Mourot, G. "Rainfall-runoff modeling for sensor diagnosis". In Proc. IFAC SAFEPROCESS'97, Hull,
761   England. 1997.

762 Boukhris, A., Giuliani, S., Mourot, G, "Rainfall-runoff multi-modelling for sensor fault diagnosis", Control Engineering Practice, vol
763   9 (6), pp. 659-671. 2001

764 Calafiore, G., Campi, M.C. and L. El Ghaoui. "Identification of Reliable Predictor Models for Unknown Systems: a Data-
765   Consistency Approach based on Learning Theory". IFAC World Congress, Barcelona, Spain, 2002.

766 Campi, M.C., Calafiore, G., Garatti, S. "Interval predictor models: Identification and reliability", Automatica, Volume 45, Issue 8. pp.
767   382-392. 2009.

768 Cembrano, G., Quevedo, J., Salamero, M., Puig, V., Figueras, J. and Martí, J. Optimal control of urban drainage systems: a case
769   study. Control Engineering Practice, 12(1), pp. 1-9, 2004.

770 Combastel, C., S. Gentil, and J. P. Rognon.. "Toward a better integration of residual generation and diagnostic decision". IFAC
771   SAFEPROCESS'03, Washington, USA. 2003.

772 Cordier, M., P. Dague, F. Lévy, J. Montmain, M. Staroswiecki, and L. Travé-Massuyès, "Conflicts versus analytical redundancy
773   relations: a comparative analysis of the model-based diagnosis approach from the artificial intelligence and automatic control
774   perspectives". IEEE Transactions on Systems, Man, and Cybernetics. Part B: Cybernetics. vol. 34, no. 5, pp. 2163–2177, 2004.

775 Chen J. and R.J. Patton. "Robust Model-Based Fault Diagnosis for Dynamic Systems". Kluwer Academic Publishers. 1999.

776 Duchesne, S., Mailhot, A., Dequidt, E., and Villeneuve, J.. Mathematical modeling of sewers under surcharge for real time control of
777   combined sewer overflows. Urban Water, 3:241-252, 2001.

778 Figueras, J., Cembrano, G., Puig, V., Quevedo, J., Salamero, M. and Martí, J. CORAL: an object-oriented tool for optimal control of
779   sewer networks. Proceedings on IEEE International Symposium on computer aided control system design, pp. 224–229, 2002.

780 Figueras, J., Puig, V., Quevedo, J. Fault Diagnosis under Multiple Sequential Faults of the Rain-Gauge Network used to Control the
781   Barcelona Sewer System. Proceedings of the 16th World Congress IFAC. Prague, Czech Republic. 2005.

782 Gelormino, M. and Ricker, N. Model predictive control of a combined sewer system. International Journal of Control, 59, pp. 793-
783   816, 1994.

784 Gertler J.J. "Fault Detection and Diagnosis in Engineering Systems". Marcel Dekker, 1998.

Guerra, P., Puig. V. "Passive Robust Fault Detection using Interval MA Parity Equations: Inverse vs Direct Image Tests". Proceedings of the 17th World Congress IFAC. Seoul, Korea. 2008.

Giuliani, S., Boukhris, A., Mourot, G. "Principles of a Rain Gauge Fault Diagnosis System for Urban Sewer Network Control". In Proc. IFAC SAFEPROCESS 1997, Hull, England, 1997.

Kóscielny, J. M. "Fault isolation in industrial processes by the dynamic table of states method," Automatica, vol. 31, pp. 747–753, 1995.

Kóscielny, J.M., Bartys, M. "Multiple Fault Isolation in Diagnostics of Industrial Processes". European Control Conferece (ECC03). Cambridge, UK.

Marinaki, M. and Papageorgiou, M. Optimal Real-time Control of Sewer Networks. Springer. 2005.

Maciejowski, J.M. "Predictive Methods in Fault-tolerant Control" in Control of Complex Systems by Aström, K.J et al. (Eds). Springer. 2001.

Ragot, J., Maquin, D. (2006). "Fault measurement detection in an urban water supply network". Journal of Process Control, Volume 16, Issue 9, Pages 887-902, 2006.

Meseguer, J., Puig, V., Escobet, T., Quevedo, J. "Sensor Fault Diagnosis using Linear Interval Observers" Workshop on Principles of Diagnosis DX'07. Nashville, TN, USA. 2007.

Meseguer, J., Puig, V., Escobet, T. "Fault Diagnosis Using a Timed Discrete-Event Approach Based on Interval Observers: Application to Sewer Networks". IEEE Transactions on Systems, Man and Cybernetics: Part A, Volume 40(5), pp. 900-916.

Milanese, M., Norton, J., Piet-Lahanier, H., Walter, E. (eds). "Bounding Approaches to System Identification". Plenum Press.H. 1996.

Nikiforov, I. "A simple recursive algorithm for diagnosis of abrupt changes in signals and systems". Proceedings of the 1998 American Control Conference, vol.3.

Ocampo-Martínez, C., Ingimundarson, A., Puig, V. and Quevedo, J. Objective prioritization using lexicographic minimizers for MPC of sewer networks. IEEE Transactions on Control Systems Technology, 16(1):113-121, 2008.

Patton, R.J., Frank, P.M. and R.N. Clark. "Issues of fault diagnosis for dynamics systems". Springer. 2000.

Pleau, M., Colas, H., Lavalle, P., Pelletier, G., and Bonin, R. Global optimal real-time control of the Quebec urban drainage system. Environmental Modelling & Software, 20:401-413, 2005.

Petti, T.F., J. Klein, and P. S. Dhurjati. "Diagnostic model processor: Using deep knowledge for process fault diagnosis," AIChE Journal, vol. 36, p. 565. 1990.

Piatyszek, E., Voignier, P. and Graillot, D. (2000). Fault detection on a sewer network by a combination of a Kalman filter and a binary sequential probability ratio test. Journal of Hydrology, Volume 230, Issues 3-4, Pages 258-268, 2000.

Ploix, S., Adrot, O. and J. Ragot. "Parameter Uncertainty Computation in Static Linear Models". 38th IEEE Conference on Decision and Control. Phoenix. Arizona. USA. 1999.

817 Puig, V., Quevedo, J., Escobet, T. Nejjari, F., S. de las Heras. "Passive Robust Fault Detection of Dynamic Processes Using Interval
818   Models", IEEE Transactions on Control Systems Technology, Volume 16, Issue 5, 1083 – 1089, Sept. 2008.

819 Puig, V. J. Quevedo, T. Escobet, and B. Pulido. "A New Fault Diagnosis Algorithm that Improves the Integration of Fault Detection
820   and Isolation" in Proccedings of ECC-CDC'05, Sevilla, Spain. 2005.

821 Schilling, W., Anderson, B., Nyberg, U., Aspegren, H., Rauch, W., and Harremes, P.. Real-time control of wasterwater systems.
822   Journal of Hydraulic Resources, 34(6):785-797, 1996.

823 Schütze, M., Campisano, A., Colas, H., Schilling, W. and Vanrolleghe, P. Real time control of urban wastewater systems: Where do
824   we stand today? Journal of Hydrology, 299:335-348, 2004.

825 Schütze, M., Butler, D. and Beck, B. Modelling, Simulation and Control of Urban Wastewater Systems. Springer. 2002.

826 Vanden Daele, R. Y. Peng and M. Kinnaert "Fault diagnosis using belief functions" in Proceedings of SAFEPROCESS'97, Hull,
827   U.K., pp 546-551, 1997.

828 Vento, J.; Puig, V.; Sarrate, R. (2010). "Fault Detection and Isolation of Hybrid Systems using Diagnosers that combine Discrete and
829   Continuous Dynamics". Conference on Control and Fault Tolerant Systems, Nice, France